

Aeroacoustic assessment of the performance of Over-Tip liners in reducing airfoil noise

Sergi Palleja-Cabre*, Brian J. Tester[†], and R. Jeremy Astley[‡]

Institute of Sound and Vibration Research, University of Southampton, Southampton, SO17 1BJ, UK

Georgios Bampanis[§]

University of Lyon, 36 Avenue Guy de Collongue, 69134 Écully, France

The reduction of fan broadband noise in the next generation of Ultra-High By-pass-Ratio (UHBR) engines remains a key technology challenge for the foreseeable future. The Over-Tip-Rotor (OTR) liner concept has been studied as a technology with the potential to further reduce fan noise and significant noise reductions have been measured. This paper describes a fundamental experimental evaluation that represents the Over-Tip-Rotor liner as a static airfoil with its tip located over a flat plate containing a flush-mounted lined insert and separated from the airfoil tip by a small gap. Differences in measured far-field sound spectra and in source power estimates derived from post-processed spiral array data have shown broadband gap noise reductions of 5-10 dB, even in the absence of a tip gap. Over-tip liners are found to suppress noise sources when located in the immediate vicinity, irrespective of the generation mechanism, mainly due to back-reaction effects on the source. An analytical prediction model for the over-tip liner noise reduction, based on a point source located over an infinite lined plane, is evaluated and compared with the experimental data. The model captures the back-reaction effects and provides qualitative agreement with the measured data, including the variation of noise reduction with increasing gap size.

I. Nomenclature

A	=	specific acoustic admittance
c	=	speed of sound
e	=	tip gap size
h	=	liner cavity depth

*Marie-Curie Early Stage Researcher and PhD candidate, Acoustics Group, Institute of Sound and Vibration Research, Sergi.Palleja-Cabre@soton.ac.uk.

[†]Principal Research Fellow, Acoustics Group, Institute of Sound and Vibration Research. Senior Member AIAA.

[‡]Professor, Fluid Dynamics and Acoustics Group, Institute of Sound and Vibration Research. Senior Member AIAA.

[§]Marie-Curie Early Stage Researcher and PhD candidate, University of Lyon, georgios.bampanis@ec-lyon.fr

Presented as Paper 2020-2608 at the AIAA AVIATION 2020 FORUM, Virtual Event, June 15–19

I	=	acoustic intensity
k	=	acoustic wave number
M_r	=	mass reactance
p	=	acoustic pressure
P	=	acoustic power
R	=	specific acoustic resistance
S_{pp}	=	power spectral density of far-field acoustic pressure
u	=	acoustic particle velocity
Z	=	specific acoustic impedance
(x, y, z)	=	Cartesian coordinates
(r, θ, ϕ)	=	spherical coordinates
α	=	normal incidence absorption coefficient
$\Delta x, \Delta y$	=	size of discretised domain cell
λ	=	acoustic wavelength
ω	=	angular frequency
Ψ	=	observation angle: azimuthal angle corrected with the angle of incidence
ρ	=	air density

Subscripts

f	=	free-field quantity
gap	=	isolated gap contribution
no-gap	=	baseline configuration without gap
total	=	measured spectra including all noise sources
x	=	axial direction
∞	=	integrated over a hemi-sphere

Superscripts

H	=	hard wall configuration
L	=	lined configuration
$*$	=	complex conjugate

II. Introduction

THE continuous growth of air traffic will require the use of innovative technologies to further reduce the levels of community noise exposure of future engines without causing a penalty in weight and CO₂ emissions. The noise signature during take-off of the next generation of Ultra-High By-pass-Ratio (UHBR) engines is predicted to be dominated by fan noise. The attenuation of fan broadband noise and the reduction of the noise sources itself remains a key technology challenge for the foreseeable future.

The sources of fan rotor-blade broadband noise can be divided into self-noise and interaction noise. The dominant source of fan self-noise is the trailing edge noise, caused by the local interaction of the eddies within the turbulent boundary layer generated on the suction surface of the fan blades with the trailing edge. Tip clearance noise can also be considered as fan self-noise, although it is not clear how significant it is among other noise sources [1]. The pressure difference between the suction side and the pressure side of the fan blades creates a jet-like flow through the tip gap that rolls up into a tip leakage vortex (TLV). The main source mechanism of tip gap noise is attributed to the interaction of the turbulent structures in the jet-like cross-flow with the blade tip suction side edge and the scattering by the tip edge and/or the trailing edge of the unsteady perturbations induced by the tip vortex [1–3]. Recent LES simulations of the experimental set-up tested in [1, 2] have shown agreement with the experiments and identified the former noise mechanism as dominant by means of an acoustic decomposition [4]. Interaction noise includes fan blade-boundary layer interaction and fan blade-outlet guide vane (OGV) interaction. The turbulent structures in the boundary layer and the fan wakes, respectively, radiate broadband noise when impinging on the leading edge of the fan/OGVs. The fan-OGV interaction, also called turbulence-impingement noise (TIN), is regarded as the dominant source of fan broadband noise [5].

Over-Tip-Rotor (OTR) acoustic treatments have been investigated during the past decade as a technology with the potential to further reduce the fan noise in turbofan engines [6–11], and noise reductions have been measured in the range of 1-5 dB inlet PWL with relatively low impact on the aerodynamic efficiency linked to the use of circumferential grooves [12, 13]. The use of grooves in the acoustic treatment can cause a noise penalty over certain frequencies at low fan speeds but has been found to be minimal at high fan speeds[11]. The noise reduction mechanism of OTR liners is usually attributed to a modification of the source itself combined with the conventional attenuation of acoustic waves propagating over the liner. A recent study [13] also shows that OTR liners can reduce the turbulence intensity in the fan wake, potentially reducing broadband fan-OGVs interaction noise by 1-2 dB. The importance of considering the coupling of the sound sources and the liner when targeting the optimum liner impedance has been highlighted in [14] for liners installed in the bypass region and in close proximity to the OGVs. Current work at the ISVR to improve the understanding of the noise reduction performance of OTR liners include the development of analytical models considering the liner-source coupling [15] and fundamental experimental studies, as described here.

The fan rotor and OTR liner are represented here by a *static* airfoil with its tip located over a flat plate containing a

flush-mounted lined insert and separated from the airfoil tip by a small gap. With this configuration, the noise reduction mechanisms related to gap noise can be studied separately from other noise source mechanisms in the engine. It also means that the measurements can be performed in an open jet, permitting the use of far-field and noise localisation measurements. Previous work on the aeroacoustic assessment of tip leakage noise sources in a similar set-up was performed by Jacob *et al.* [1] and Grilliat *et al.* [2], who showed that the incoming flow combined with the camber of the airfoil and its angle of attack, creates a jet-type cross-flow through the tip gap that resembles the noise generation mechanism of a tip vortex. This idea is used here to assess the performance of acoustic liners in reducing such noise source mechanisms, either by modifying the source and/or attenuating the noise as it propagates over the liner, and to relate the findings to OTR acoustic treatments. The low-speed flow regimes and relatively large tip gaps used in this experiment do not correspond to realistic operating conditions in a turbofan engine and does not include cascade effects or non-linearities. However, it captures a key element of the noise reduction of over-tip liners, that of the radiation of noise from an aerodynamic source in very close proximity to a liner and to a blade tip, albeit both stationary, but in the presence of flow, and reveals some aspects of the liner attenuation and source modification for this canonical problem. The performance of Over-Tip liners in suppressing airfoil noise sources in the absence of a tip gap, such as trailing edge noise, is also explored. The analysis is based on differences in measured far-field sound spectra combined with spiral microphone array localisation techniques to quantify the contribution of each source region to the measured noise spectra. This experimental approach has been recently applied to characterise the noise sources in a swept airfoil with a free tip in [16].

The structure of this paper is as follows. In Section III the experimental set-up and the Over-Tip liner are described. The gap noise generation and the liner noise suppression for a fixed test case are analysed in Section IV and Section V using differences in far-field sound spectra and in radiated source power respectively. A parametric study is described in Section VI, which includes the scaling with free-stream velocity, the effect of gap size, the use of different liner configurations and of trailing edge feathers. A comparison of the experimental results with a simple analytical point source model is described in Section VII.

III. Experimental set-up

A. Wind-tunnel set-up, airfoil and Over-Tip liner

The acoustic measurements presented in this paper were performed in the low-speed open-jet anechoic wind tunnel of Ecole Centrale de Lyon (ECL), which has been described in detail elsewhere [17, 18]. A rectangular nozzle with a vertical exit cross-section of 15 cm x 30 cm delivers a clean uniform flow with turbulence intensity of 0.3% [19], at velocities ranging between 19 m/s to 32 m/s, into an anechoic chamber of 4 m x 5 m x 6 m. The contraction ratio of the nozzle is 2:1 from an initial section of 30 cm x 30 cm. A cambered airfoil NACA 6512-10 with a chord of $c = 13$ cm is

held vertically between two horizontal plates. The upper end of the airfoil is placed in a slit disc inserted in the upper plate such that the angle of attack can be varied by rotating the disc and the gap adjusted by simply slipping and locking the airfoil in the upper disc. The camber of the airfoil and relatively high angles of attack enhance the cross-flow in the tip region and the formation of a tip vortex. A hard wall or a liner insert was flush mounted in the lower support, in direct contact with the cross-flow within the gap. The set-up with and without the airfoil is shown in Fig. 1a-1b.

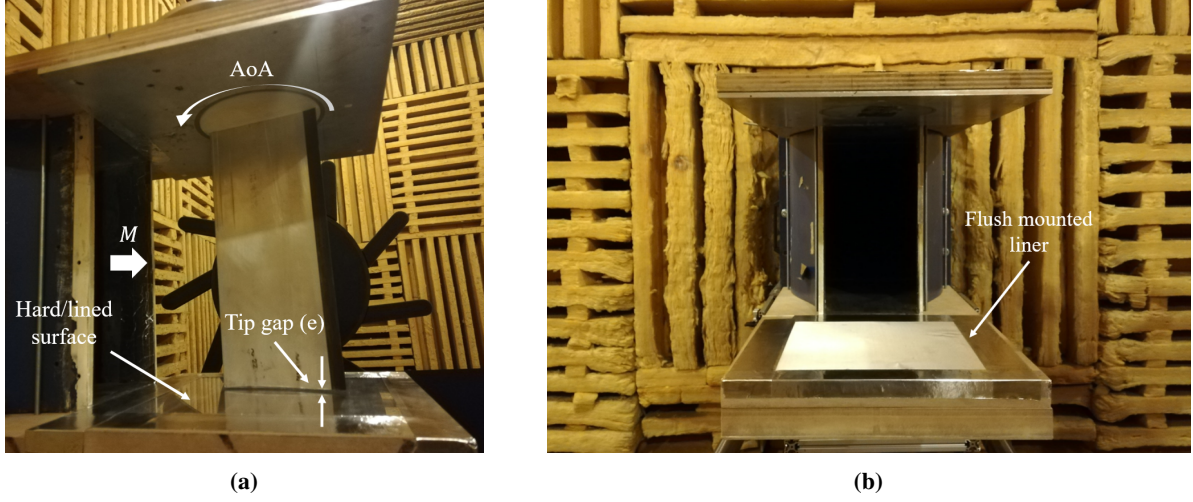


Fig. 1 Over-tip liner test set-up: (a) Full set-up and (b) Support plates with a flush mounted liner.

Simple SDOF cavity liners were used in this instance so that well-established models could be used to predict the liner acoustic impedance. Non-linear effects were not expected due to the low sound pressure levels incident on the liner inserts. Three wire meshes of different acoustic resistance were bonded directly to a honeycomb structure with a cavity depth of $h=2$ cm using spray adhesive to minimise blockage. The smooth wire meshes provide minimal interaction with the open-jet flow, hence reducing the impact of aerodynamic effects in the current study. Impedance tube tests of liner samples were performed using a Bruel & Kjaer two-microphone impedance measurement tube type 4206. Curve fitting of the results to Eq. 1 [20], where k is the wavenumber, gave values of resistance (R) and mass reactance (M_r) shown in Table 1. The measured impedance and normal incidence absorption coefficient (Eq. 2) and the corresponding fitted curves are shown in Fig. 2. The notation $e^{j\omega t}$ is used here.

$$Z = R + j [M_r k - \cot(kh)] \quad . \quad (1)$$

$$\alpha = \frac{4R}{(R+1)^2 + [M_r k - \cot(kh)]^2} \quad . \quad (2)$$

Table 1 Specific acoustic resistance and mass reactance of each liner configuration.

Liner ID	4	5	7
R	1.11	0.36	1.47
M_r	0.47 cm	0.30 cm	1.83 cm

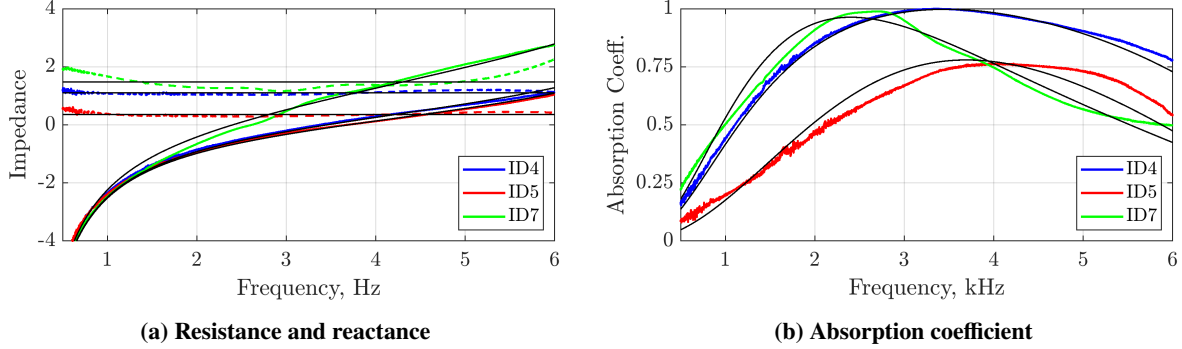


Fig. 2 Characterisation of over-tip liner impedance. In (a) dashed lines are the specific acoustic resistance and solid colour lines the specific acoustic reactance. In both figures the black lines are the curve-fitted values.

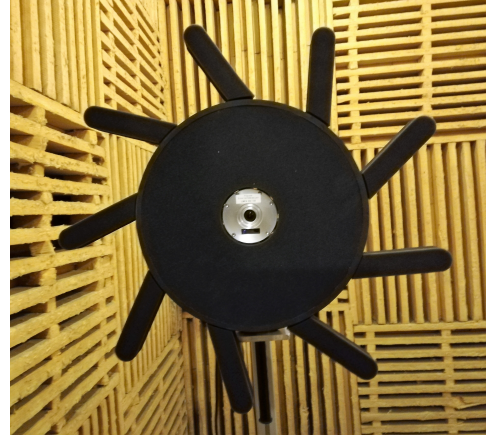
B. Far-field and spiral microphone array

The acoustic far-field was measured on a portion of a sphere with coordinates (r, θ, ϕ) employing a rotating vertical arc of six microphones B&K 1/2" type 4189, equally spaced along the arc from $\phi = 0$ deg. (mid-span plane) to $\phi = 75$ deg., as shown in Fig. 3a. The array, of a radius of $r = 1.25$ m, was aligned with the airfoil LE and is fixed to a remote-controlled rotating table to modify the azimuthal angle θ of the meridian plane. Appropriate values of ϕ and θ were used to minimise the noise scattered from the support plates and the hydrodynamic pressure of the wind-tunnel jet respectively. Spurious reflections or scattering measured on the microphones due to the components of the arc array itself are addressed by the spectral difference procedure described in Section IV. All far-field acquisitions were made with an external unit PXI-036, averaging over 30 samples of 1 second, with a sampling frequency of 51.2 kHz and a bandwidth of 1Hz over the frequency range 0-25.6 kHz.

The spiral microphone array shown in Fig. 3b, consisted of 81 sensors and was located 0.55 m away from the airfoil and parallel to the flow direction. The mean polar-azimuthal array aperture is about 48 deg. relative to the mid-span and leading edge position of the airfoil. The post-processing technique to localize the noise sources and provide relevant power level spectra for each source is based on a deconvolution algorithm called CIRA, implemented in LMS software under a MicrodB license; a description of the CIRA method can be found in [21]. The practical aspects concerning the low-frequency spatial resolution limits and the correction for the apparent flow displacement caused by the flow convection have been addressed in [18].



(a) Far-field microphone arc array [18]



(b) Spiral microphone array as viewed from the airfoil

Fig. 3 Far-field and spiral microphone arrays used in the experiments.

IV. Differences of Far-Field Sound Spectra for hard/lined configurations

The quantification of the noise reduction of a particular airfoil-noise source mechanism in the presence of other background noise and additional sources has to be treated carefully to avoid misleading noise reduction spectra, as noted in [16–18]. The background noise sources include noise radiating from the wind tunnel upstream of the contraction, the noise generated by the flow at the edges of the nozzle, noise diffraction at the edges of the support plates and jet mixing noise. Therefore, to isolate airfoil-noise sources, the background noise contribution is assumed to be uncorrelated with the airfoil noise and is removed by subtracting the dimensional noise spectral density measured *without* airfoil from the total sound spectral density *with* the airfoil.

To measure the reduction of gap noise using an over-tip liner, it is necessary to separate the contributions of gap noise from that of trailing edge noise (TEN) in the total measured spectra. To measure the contribution of TEN, a zero-gap hard/lined baseline case is used (i.e. where gap noise is absent). The gap noise contribution ($S_{pp,gap}^{H/L}$) is obtained by subtracting the dimensional noise spectra of the baseline case ($S_{pp,no\ gap}^{H/L}$) from the total measured spectra ($S_{pp,total}^{H/L}$), i.e.

$$PSD_{gap}^{H/L} = 10 \log_{10} \left(S_{pp,gap}^{H/L} \right) = 10 \log_{10} \left(S_{pp,total}^{H/L} - S_{pp,no\ gap}^{H/L} \right) . \quad (3)$$

The subtraction is performed *both* for the hard (H) and lined (L) configurations and the procedure already removes background noise sources. This procedure is impossible when airfoil noise sources are masked by the background noise or if the airfoil noise sources have similar contributions to the overall sound field [16]. In those circumstances, microphone array localisation techniques can provide a means of quantifying the contribution of each noise source, as detailed in Section V. The analysis bandwidth of the far-field measured auto spectral densities (S_{pp}) has been set to 32/64 Hz to avoid the large high-frequency scatter due to statistical errors. The reduction of gap noise (PSD_{gap} IL) and total noise (PSD_{total} IL) is obtained following Eq.4-5.

$$\text{PSD}_{\text{gap IL}}(\text{dB}) = \text{PSD}_{\text{gap}}^{\text{H}} - \text{PSD}_{\text{gap}}^{\text{L}} = 10 \log_{10} \left(S_{pp, \text{gap}}^{\text{H}} \right) - 10 \log_{10} \left(S_{pp, \text{gap}}^{\text{L}} \right) \quad . \quad (4)$$

$$\text{PSD}_{\text{total IL}}(\text{dB}) = \text{PSD}_{\text{total}}^{\text{H}} - \text{PSD}_{\text{total}}^{\text{L}} = 10 \log_{10} \left(S_{pp, \text{total}}^{\text{H}} \right) - 10 \log_{10} \left(S_{pp, \text{total}}^{\text{L}} \right) \quad . \quad (5)$$

This experiment presents a multi-variable problem: (1) the gap size, (2) the angle of attack (AoA), (3) the flow speed (M) and (4) the impedance of the hard/lined insert. The results presented in this section and Section V are limited to a fixed gap size of $e = 5$ mm, AoA = 18 deg. and $U = 27$ m/s for a hard wall reference case and two liner configurations (ID4-5). The baseline case required to isolate the gap noise in each configuration is performed for $e = 0$ mm, AoA = 18 deg. and $U = 27$ m/s. All far-field results presented here have been obtained from the mid-span microphone of the arc array and on the pressure side of the airfoil, that is $(\phi, \theta) = (0, -90)$ deg.. Note that the spiral array used for the source localization and extraction procedure of Section V is located on the suction side of the airfoil.

The total PSD measured for a selection of cases is shown in Fig. 4a. Small variations between the baseline (hard + no gap) and reference (hard + gap) cases can be observed up to 5 kHz. That is, below this frequency the spectra is dominated by TEN, whereas above 5 kHz gap noise becomes significant. A discussion on the physical mechanisms of gap noise, which also includes TEN, is given in Section VI. The resulting PSD gap noise spectra for the hard wall and lined cases after the subtraction of the TEN and background noise are shown in Fig. 4c. At those frequencies where TEN dominates over gap noise the difference of S_{pp} with and without gap can be very small, resulting in zero or negative values after the subtraction and hence does not permit an accurate assessment of the gap sources at those frequencies. This is less of a problem for frequencies higher than 5 kHz, where the gap noise spectra for the hard and lined cases can be isolated. However, high variability in the isolated gap noise spectra for the lined configurations is observed over 12-15 kHz and 18-20 kHz due to, effectively, measuring the background noise with and without the gap. Although these higher frequencies are not relevant for turbofan engines, the measured spectra over these frequencies are dominated by gap noise and therefore useful to compare with the prediction model in Section VII.

The noise reduction due to the over-tip liners, the PSD Insertion Loss (PSD IL), is now derived by taking the difference, in dB terms, of the PSD levels in Fig. 4c, as indicated in Eq. 4. The resulting gap noise reduction spectra and the normal incidence absorption coefficient for each liner are shown in Fig. 4b and Fig. 4d respectively. Three humps can be observed in the noise reduction spectra that can be broadly related to the resonances and anti-resonances of the liners. The normal incident absorption curves show two anti-resonances at 8.5 kHz and 17 kHz, with peak noise reduction around 11 kHz and 19 kHz. Although the $\text{PSD}_{\text{total IL}}$ achieved with liner ID4 is generally around 1 dB higher than with liner ID5 (Fig. 5), as expected from the magnitude of the absorption coefficient curves, the subtraction procedure forces the two $\text{PSD}_{\text{gap IL}}$ spectra to collapse. The results of this section show that over-tip liners can provide broadband PSD gap noise reduction of 5-10 dB (Fig. 4b), corresponding to 2-3 dB of PSD total reduction (Fig. 5).

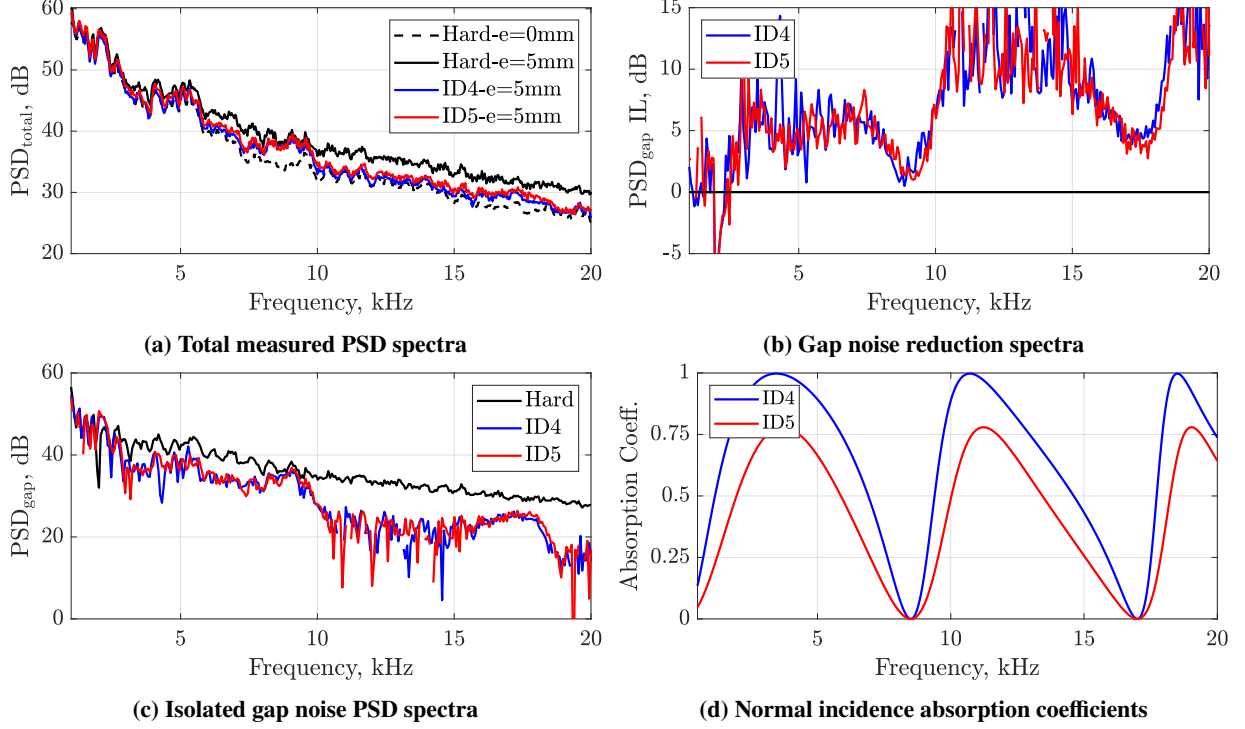


Fig. 4 Measured PSD noise spectra and over-tip liner noise reduction performance.

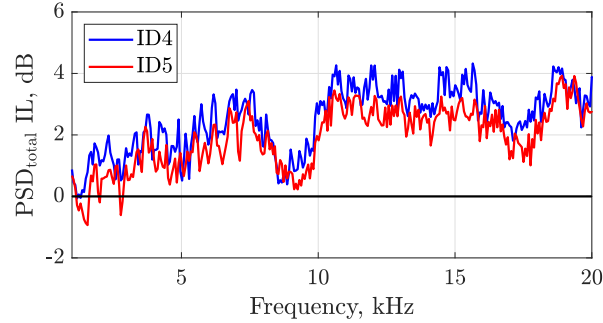


Fig. 5 Total PSD noise reduction spectra.

V. Noise localisation and extraction

Equivalent sound power maps can be obtained for each test case and prescribed frequency range by using the data acquired with the spiral array and the CIRA post-processing technique, which assumes that the sources are uncorrelated monopoles. However, the power here is defined as the monopoles source powers integrated over the source region that is then radiated into the aperture of the spiral array and not the total power radiated over the sphere surrounding the airfoil. The sources of acoustic power can be defined as selected spatial areas or regions of interest, such as the trailing and leading edge of the airfoil or the gap region, to obtain the spectrum of the power radiated by the sources within that region, subject to the usual resolution limits of the spiral array. That is, it provides a means of quantifying the contribution of each noise source region.

The results in this section are limited to the zero-gap baseline (hard and lined with ID4) and the hard wall reference and liner ID4 configurations with a tip gap as described in Section IV. The equivalent sound power maps for these cases are shown in Fig. 6 for three ranges of frequencies of interest based on the analysis of the far-field data: $f=[4-6]$ kHz, which is expected to be dominated by TEN; $f=[6-9]$ kHz, where both noise sources may have a prominent role and should capture the first hump of the over-tip liner noise reduction; and $f=[9-12]$ kHz, which is expected to be dominated by gap noise and capture the second hump of liner noise reduction. Note that in all the PWL maps the nozzle is located on the right hand side of the image and the flow goes from right to left.

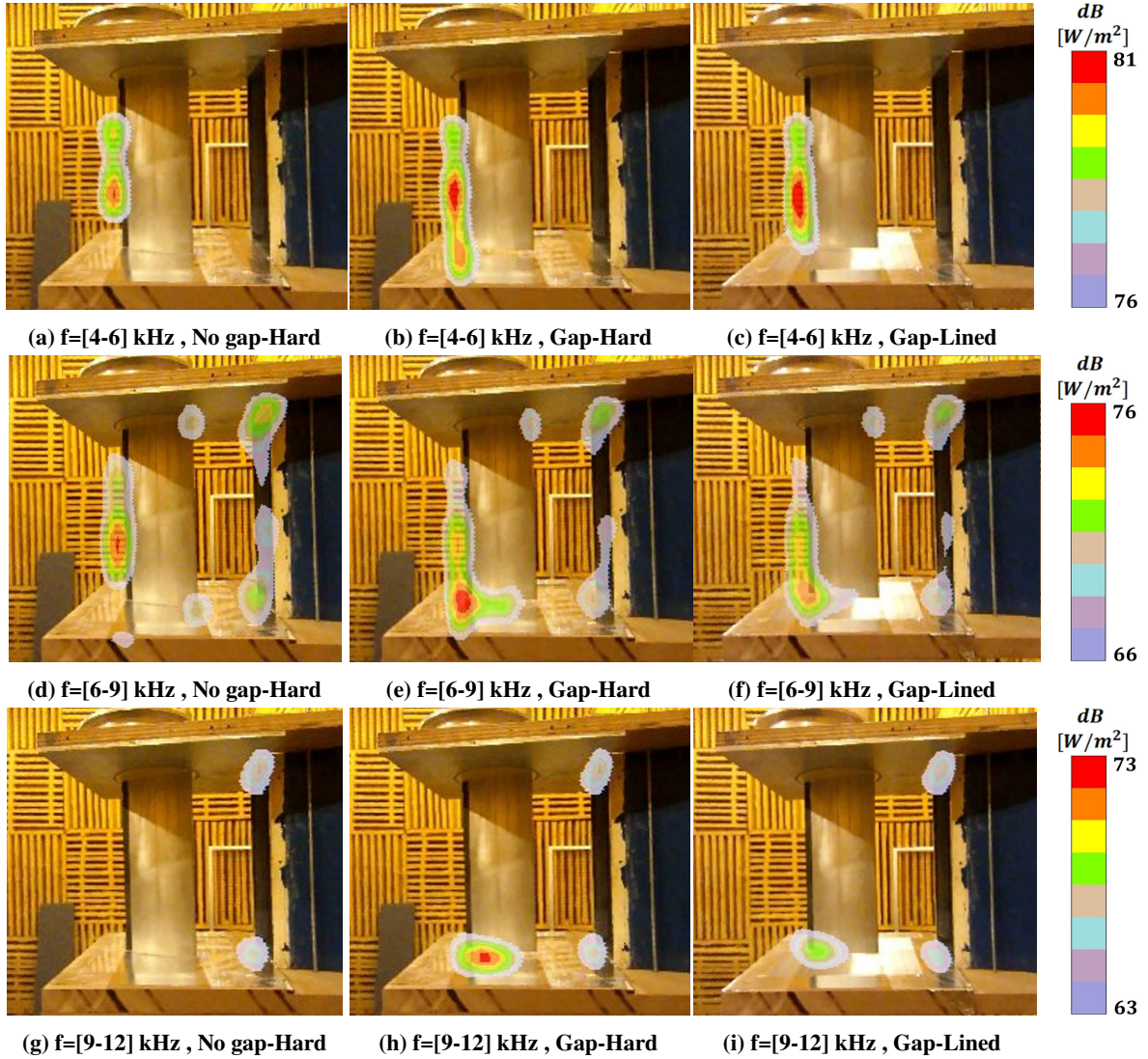


Fig. 6 PWL maps for the baseline, reference and lined cases for the frequency ranges of (a)-(c) $f=[4-6]$ kHz, (d)-(f) $f=[6-9]$ kHz and (g)-(i) $f=[9-12]$ kHz.

Starting with Fig. 6a, it can be observed that with no gap the dominant source is TEN centred around the mid-span of the airfoil. A TE contribution towards the tip of the airfoil can be observed when a tip gap is introduced (Fig. 6b),

which is attenuated locally in the vicinity of the liner (Fig. 6c). A similar trend can be observed for the range of $f=[6-9]$ kHz, although the dominant sources when the gap is present are now shifted towards the tip of the airfoil around the TE (Fig. 6e). The over-tip liner mitigates the noise sources in the gap region but does not affect the TEN radiated from span sections located further away, as shown in Fig. 6f. In the third frequency range, the no gap baseline only shows weak sources generated at the nozzle exit (Fig. 6g). However, with a tip clearance, the noise sources are much better defined and localized within the gap (Fig. 6h) and are strongly reduced in the presence of the over-tip liner (Fig. 6i). It is clear that at this frequency range the sources located in the gap region are dominant.

The definition of the domains for source power extraction is not obvious due to the close proximity of gap noise and TEN, especially relevant at those frequencies around the threshold where TEN or gap noise are the dominant sources. A compromise is made by selecting the gap region and a small part of the TE, here called 'GAPB' for GAP-box, and *the rest* of the TE, called 'TENB'. It should be noted that TEN is the acronym for Trailing Edge Noise, and TENB is the name for the integration area or box containing most of the trailing edge. The two areas are defined in red and green respectively in Fig. 7a. The power from the full domain and the equivalent integrated power in each area is shown in Fig. 7b-7d. The variation in the PWL from TENB between the different configurations is insignificant (Fig. 7d), showing that the noise sources in most of the TE are independent of the gap flow or the liner and confirms the choice of integration areas. As expected, the PWL spectra in the GAPB are significantly affected by the problem variables (Fig. 7c). An anomalous behaviour on the power extraction results from GAPB is observed around 2-3 kHz for the lined configurations. The analysis of the results at those frequencies will be drawn from the full domain power spectra of Fig. 7b, which show the same trends as in GAPB but to a lesser extent due to the additional contribution of TEN.

An estimation of how much additional noise is generated due to the tip leakage flow can be obtained by using the power extraction technique, i.e. by subtracting the PWL from GAPB and from the full domain with and without the gap, i.e.

$$\Delta \text{PWL}^{\text{H/L}}(\text{dB}) = \text{PWL}_{\text{gap}}^{\text{H/L}} - \text{PWL}_{\text{no-gap}}^{\text{H/L}} . \quad (6)$$

This operation can be performed both for the hard and lined configuration to assess whether the presence of the liner affects the noise generation mechanisms. The results shown in Fig. 8 and 9 have been filtered with a Savitzky-Golay filter to smooth the data while maintaining the general trends.

Ignoring the peaks in the lined results from GAPB, it can be observed in Fig. 8 that the noise generated due to the tip leakage flow affects the whole range of frequencies but is particularly pronounced in the gap region in the range of 6-12 kHz. In this frequency range, it provides an additional 8-18 dB (Fig. 8a) that accounts for 2-3.5 dB over the full domain (Fig. 8b). However, it does not vary significantly between the hard wall and the lined configurations and indicates that the noise generation mechanisms are not modified by the presence of the over-tip liner, at least up to 9

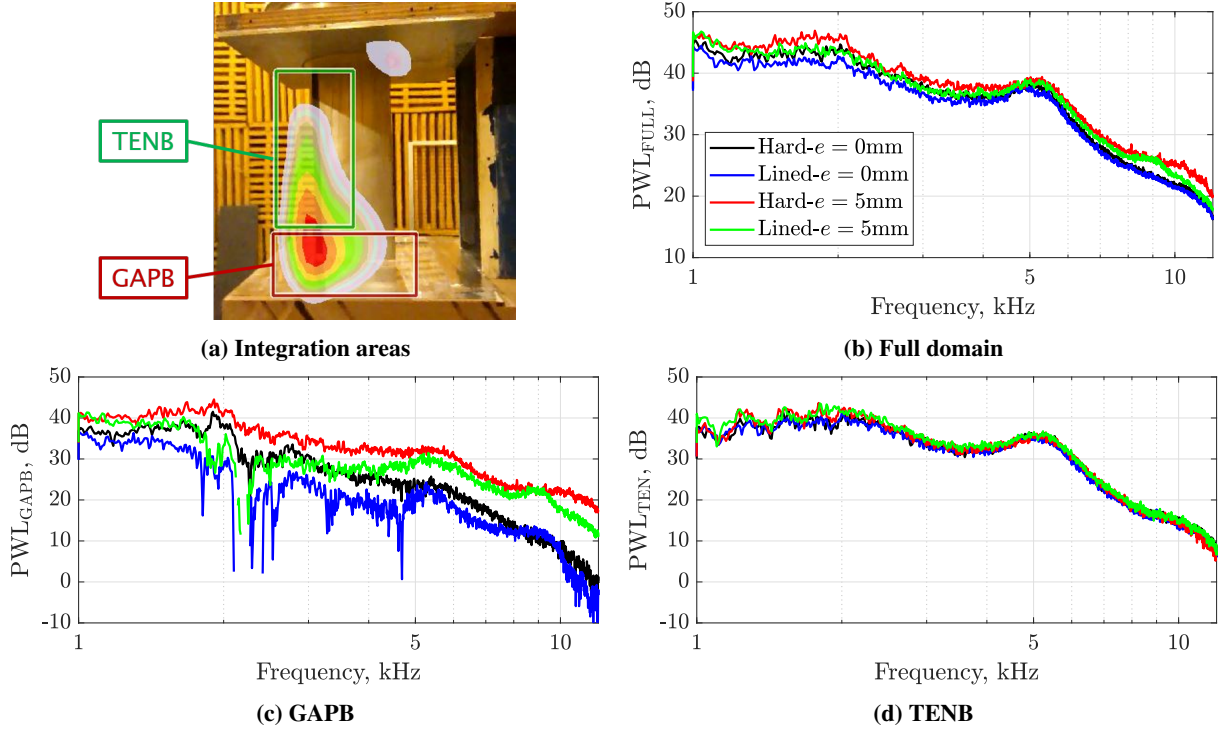


Fig. 7 (a) Definition of the integration areas and (b)-(d) power extracted in different areas.

kHz. This could be linked to the smooth wire mesh used for the liner not interfering with the aerodynamics on the tip region, selected for this purpose, as opposed to some grooved concepts used in the literature for OTR liners in fan rigs [9–11] where the interaction of the grooves and the grazing flow can result in additional noise sources [13]. The full domain PWL in Fig. 8b suggest that the noise generation above 9 kHz is lower in the lined configuration, which may not have been captured in the GAPB due to the low signal levels. Note that this procedure and analysis are based on differences of PWLs: although the trends are the same with a hard or lined insert, the absolute values are smaller in the lined configuration as shown in Fig. 7b-7c.

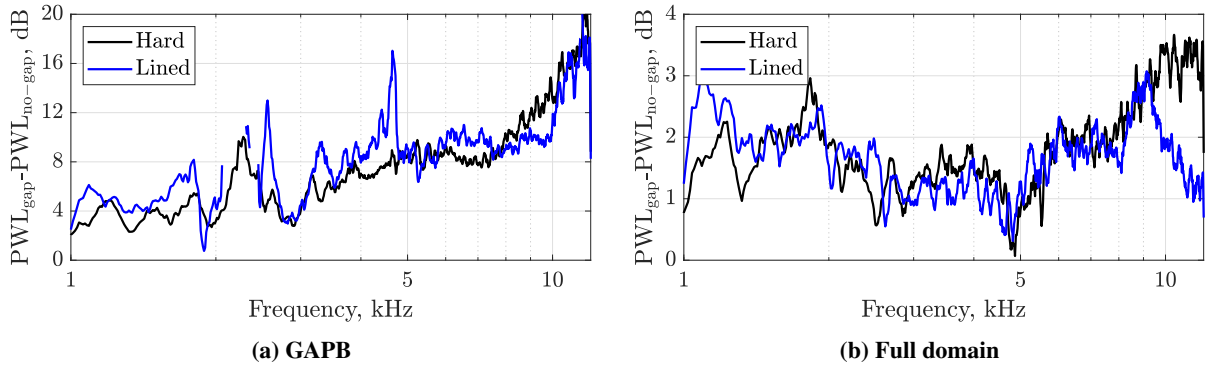


Fig. 8 Quantification of the gap noise generated by the tip leakage flow with the hard wall and the liner insert.

In the same way, the difference between the PWL for a given gap size (zero or 5mm in this section) and hard or lined

insert quantifies the noise reduced by the over-tip liner (Eq. 7), as shown in Fig. 9a and Fig. 9b for the GAPB and the full domain respectively. Similar trends to those obtained by differences of the far-field sound spectra are observed here for frequencies above 5 kHz: the anti-resonance at 8.5 kHz with null noise reduction and a peak PWL IL around 11 kHz. This approach also gives insight in the frequency range of 3-5 kHz, where both TEN and gap noise are of similar strength and far-field differences not reliable, showing that the liner can provide broadband peak PWL IL in the gap area of up to 5 dB, accounting for 1-2 dB in the full domain. The performance of the over-tip liner is not significantly modified by the tip-leakage flow, i.e. small variation with or without a gap, which suggests that the liner suppresses the noise sources located in its vicinity whether they are TE or gap noise sources. The noise reduction in the absence of tip gap shows the potential of over-tip liners in turbo-machinery applications even if the role of gap noise is not fully quantified.

$$\text{PWL IL(dB)} = \text{PWL}_e^H - \text{PWL}_e^L \quad . \quad (7)$$

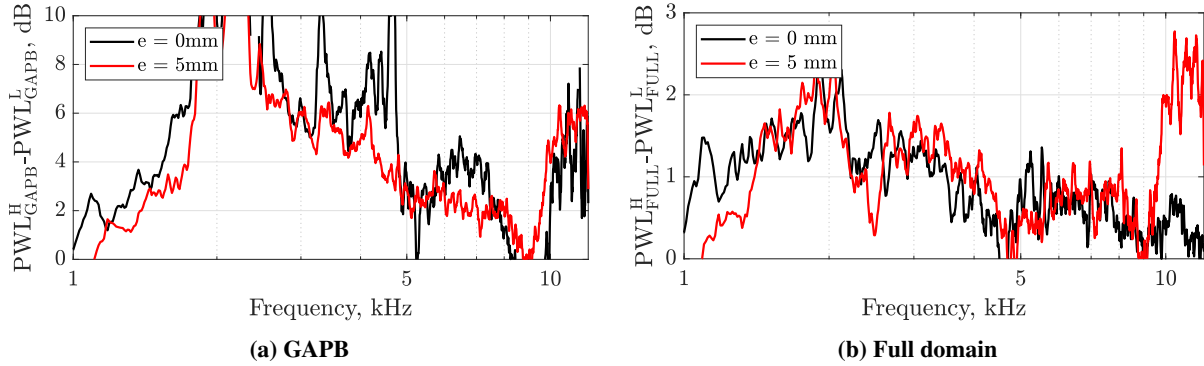


Fig. 9 Measured Over-tip liner PWL noise reduction with and without tip gap.

VI. Parametric studies

A. Scaling laws

The baseline ($e = 0$ mm, AoA=18 deg., hard/liner ID4), reference ($e = 5$ mm, AoA=18 deg., hard) and lined ($e = 5$ mm, AoA=18 deg., liner ID4) configurations have been tested at three different speeds, namely [S1 S2 S3]=[17 27 32] m/s. Previous work on the aeroacoustics of tip leakage flow [1, 2] suggests two physical mechanisms of noise generation of similar magnitude: (1) the interaction of turbulent eddies in the cross-flow and TLV with the suction side edge and the trailing edge, which varies according to the 5th power of the free-stream velocity and (2) secondary eddies in the jet-like cross-flow that radiate with a power of the free-stream velocity of 7 to 8.

The isolated gap noise (PSD_{gap}) for $S=[S1, S2, S3]$ has been plotted against the Strouhal Number based on the free-stream velocity and the airfoil chord in Fig. 10. The data in Fig. 10 was acquired with the mid-span microphone of the arc array and in the pressure side of the airfoil ($(\phi, \theta) = (0, -90)$ deg.). As noted previously, gap noise cannot be

accurately isolated at low frequencies and therefore the spectra in terms of Strouhal number is less reliable for lower flow velocities. However, at the frequencies where gap noise is dominant, the curves collapse when scaling with the 5th power of the free-stream velocity (Fig. 10a). This is not the case with the power of 7 or 8, the later shown in Fig. 10b. These results suggest that the interaction of turbulence with the tip edges is the dominant source of gap noise for the whole frequency spectrum in the current tests. The low Mach number of the experiments reported here ($M=[0.05-0.1]$) in comparison to the $M=0.2$ used in [1, 2] may cause the masking of any jet-like noise radiation.

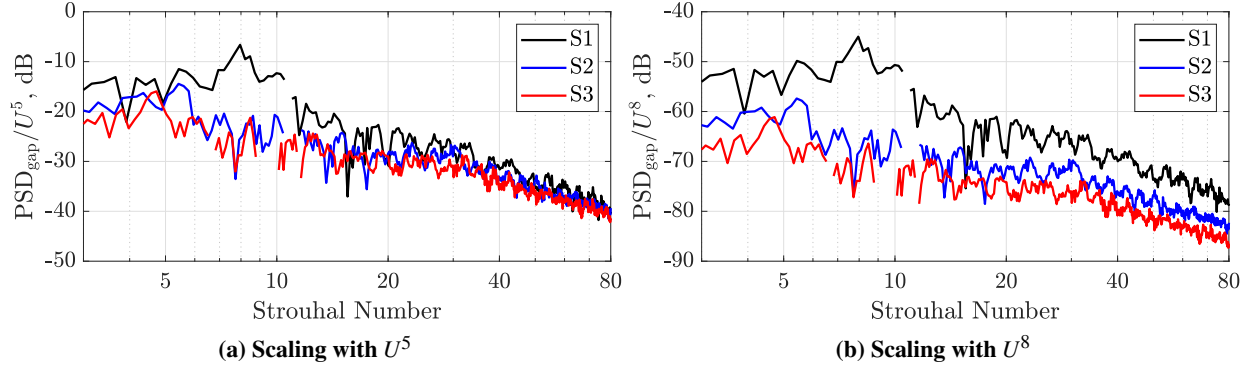


Fig. 10 Scaling of gap noise with the free-stream velocity U .

Far-field measurements have been performed for a range of meridian positions of the microphone arc array to assess the directivity pattern of gap noise and the noise reduction performance of the over-tip liner. The isolated gap noise spectrum for $U = 32$ m/s measured at the various meridian positions is shown in Fig. 11a with respect to the Strouhal number. The observation angle ($\psi = \theta + \text{AoA}$) is the azimuthal angle (θ) corrected with the angle of incidence of the airfoil (AoA), i.e. the angle relative to the chord. This plot can be compared like to like with Fig. 11 of [1] by scaling the latter using the Strouhal number. In both tests, a dipole-like directivity attributed to TE noise can be observed for $\text{St}=[1-6]$, which is stronger in the suction side possibly due to a thicker boundary layer. However, no symmetry between the pressure side and suction side can be observed at higher frequencies, showing a discrepancy with the results in [1] and stronger radiation of the gap sources towards the pressure side in this instance.

The $\text{PSD}_{\text{total}}$ noise reductions by the over-tip liner at each observation angle is shown in Fig. 11b. The same trends can be observed in the suction and pressure side of the airfoil, although the magnitude of the reduction is higher in the latter. The three humps of noise reduction discussed in the preceding sections are consistent for all measured angles. The bands of anti-resonance centred in 8.5 kHz and 17 kHz are noticeable for $\text{St} \sim [40, 80]$ respectively. The progressive increase of noise reduction with the observation angle can be linked to the amount of lined surface over which the waves travel from the source to the receiver. Given the geometry of the liner and the far-field array and assuming that the dominant sources are located close to the TE, for $\text{AoA}=18^\circ$, higher observation angles correspond to longer distances travelled over the lined surface.

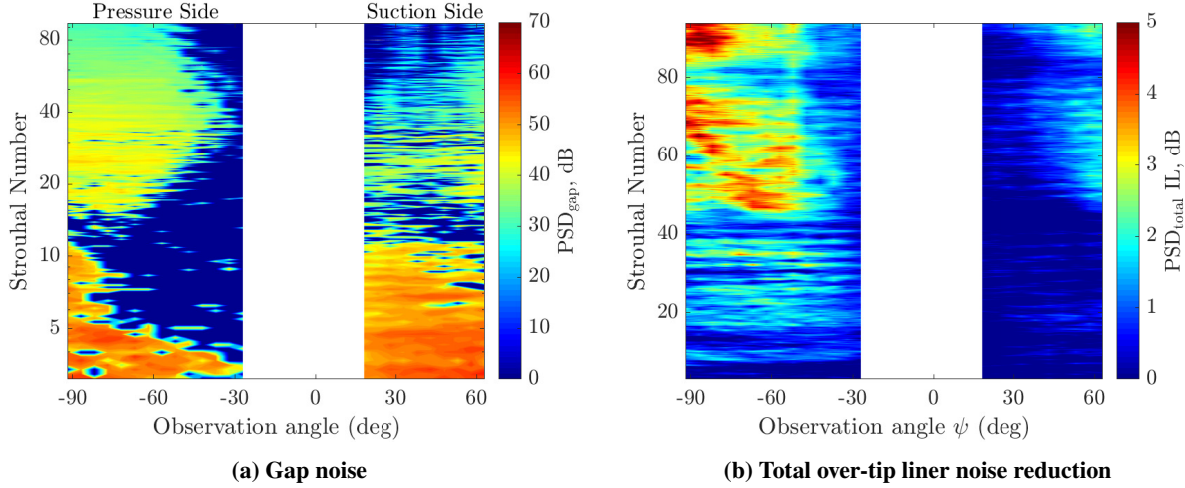


Fig. 11 Directivity of (a) gap noise and (b) total over-tip liner noise reduction.

B. Effect of gap size

The effect of the gap size on the tip-leakage noise and in the over-tip liner noise reduction performance is discussed in this part of the section. The discussion is based on far-field measurements acquired at $(\phi, \theta) = (0, -90)$ (pressure side) and $(\phi, \theta) = (0, +45)$ (suction side) for S3, AoA=18 deg., hard/liner ID4 and a range of gap sizes $e = [4 : 3 : 25]$ mm. Measurements with the spiral array were taken simultaneously and the resulting extracted power is used to extend the discussion to the GAPB area, which has been shifted upwards in accordance with the gap size.

The spectrum of the additional noise due to the gap ($\Delta \text{PSD}_{\text{total}} = \text{PSD}_{\text{total}}^{\text{gap}} - \text{PSD}_{\text{total}}^{\text{no-gap}}$) in the hard wall case is shown in Fig. 12a and 12b for the pressure side and the suction side respectively. The trends of the noise increase with the gap size vary across the spectrum but can be broadly divided into three groups: $f = [2-6]$ kHz, $f = [6-12]$ kHz and $f = [12-20]$ kHz, which apply both in the pressure side and the suction side of the airfoil. The integrated spectrum for each frequency range and gap size is shown in Fig. 12c-12e. An increase of noise followed by saturation is observed in the first frequency range ($f = [2-6]$ kHz). This is what the authors expected: a higher velocity of the cross-flow and a consequent noise rise until the gap size is big enough such that it behaves as a free tip vortex. Noise localization maps for this frequency range and S3 have shown that although TEN remains of the same magnitude as gap noise for low gap sizes, the dominant sources are shifted towards the airfoil tip TE as the gap is increased and eventually saturate in accordance to Fig. 12c. The second frequency range ($f = [6-12]$ kHz), for which gap noise is dominant, does not present any saturation at the higher gap sizes but a monotonic increase of additional noise. In contrast, the noise sources at the higher frequencies ($f = [12-20]$ kHz) are quite insensitive to the gap size. The trends outlined above agree with the quantification of additional noise from the GAPB shown in Fig. 14a. This parametric study suggests that not two but possibly three different tip-leakage noise generation mechanisms are present in the current tests. Measurements of the unsteady pressure fluctuations on the airfoil surface and of the flow in the vicinity of the tip could provide more insight

into the noise generation mechanisms and complement the discussion presented here.

The noise reduction of the over-tip liner is presented in an analogous format in Fig. 13 and Fig. 14b, the former based on the far-field measurements and the latter on the PWL extraction from the GAPB. The resonances and anti-resonances of the over-tip liner can once again be observed for the full range of gap sizes and have been used to define the integration bands of Fig. 13c-13e. In the second and third frequency bands, the dominant noise sources were found to be located at the tip of the airfoil and consequently they move away from the lined surface as the gap size is increased. As a result, the PSD IL is reduced with gap size as observed in Fig. 13d-13e for $\theta = -90$ deg. and to a lesser extent for $\theta = +45$ deg.. This trend is clearer for the isolated gap noise from GAPB shown in Fig. 14b and has been predicted with an analytical model of a point source over an infinite lined surface described in Section VII (Fig. 22). In the first frequency band, the same trend can be observed for gap sizes higher than $e=10$ mm, for which power maps (not included here but shown in [22]) indicate the dominant sources are shifted towards the airfoil tip TE. However, the increase of PSD IL at lower gap sizes over this first frequency band is less clear. It could be linked to a predicted shift and increase of the peak of noise reduction towards lower frequencies with gap size (Fig. 22) affecting the frequencies between 1-3 kHz, 8.5-10 kHz and 17-18 kHz.

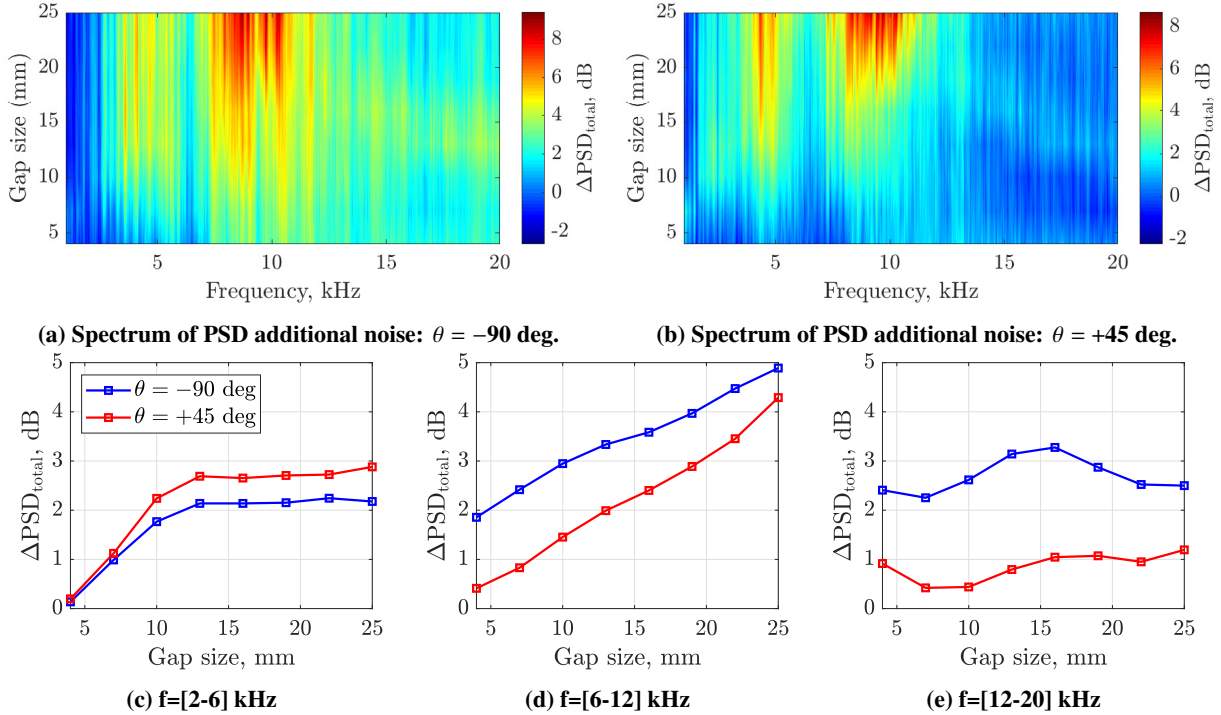


Fig. 12 Spectrum of PSD additional noise for different gap sizes and integration for discrete frequency ranges.

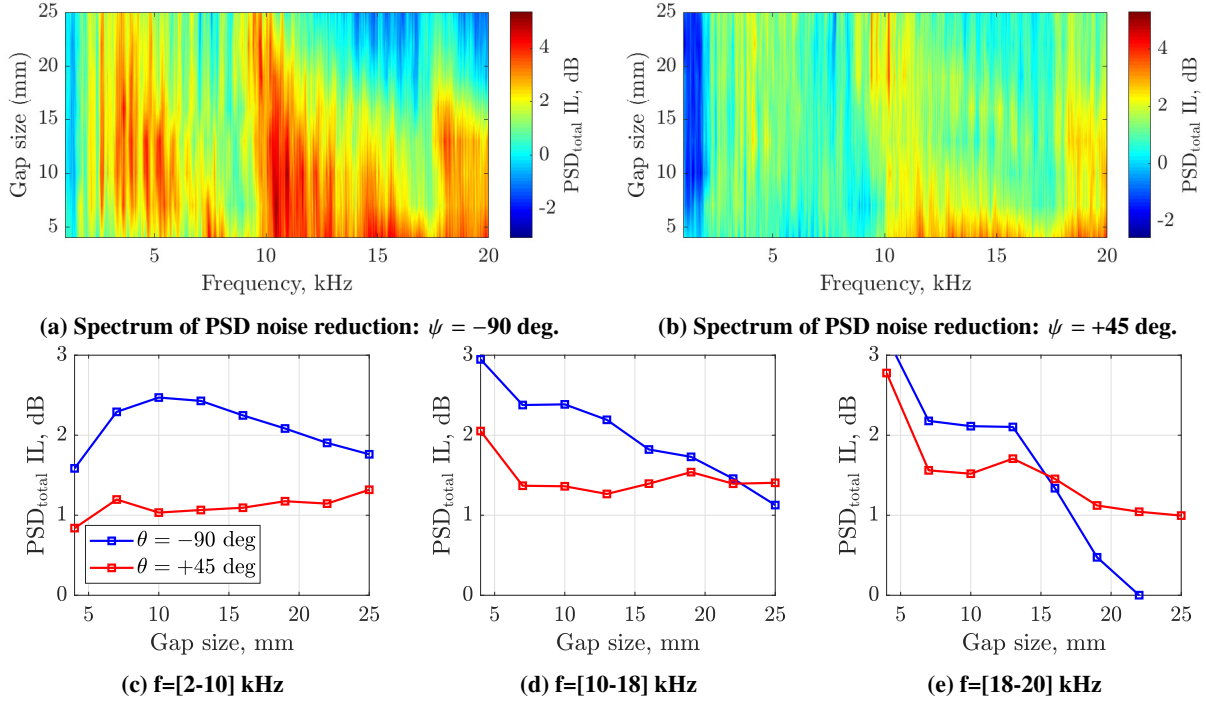


Fig. 13 Spectrum of PSD noise reduction for different gap sizes and integration for discrete frequency ranges.

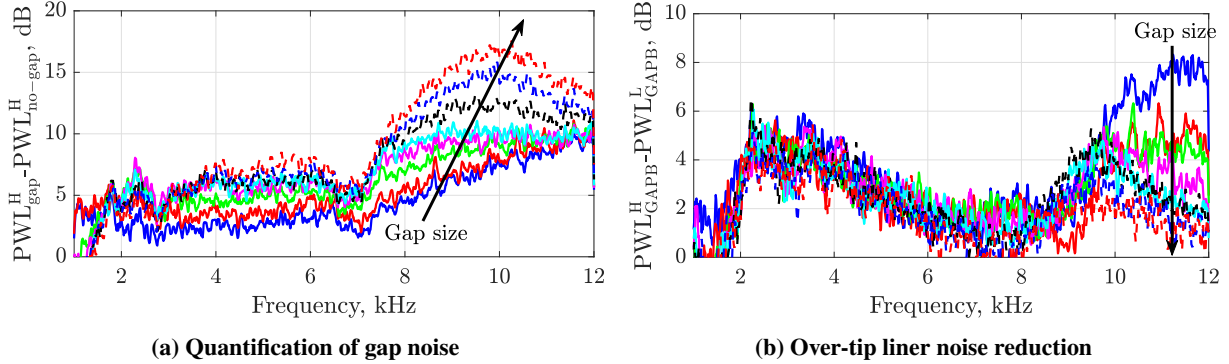


Fig. 14 Quantification of the gap noise generated by the tip leakage flow and PWL noise reduction by the over-tip liner in GAPB.

C. Source modification tests

The literature on OTR acoustic treatments [6–11] suggests that the noise reduction mechanisms of OTR liners are a combination of source modification and conventional attenuation of acoustic waves propagating over the liner. The results presented here are aimed at providing a better understanding of the relative strength of these mechanisms for this particular experimental configuration. Five different liner configurations were tested using both the far-field and the spiral arrays. Although the results presented here are based on the far-field array data, the same conclusions can be drawn from results based on the spiral array data (with the sound power extraction technique). A plan view of each liner insert with the location of the aerofoil is depicted in Fig. 15. The full liner ID4 was partially covered with a rigid

hard wall surface, flush mounted to minimise noise attenuation over certain areas. The shaded and light areas of the liners in Fig. 15 represent the lined and hard wall areas respectively. The logic behind this selection is that the ‘local’ liner should only reduce sound in the near field of the source, whereas the ‘remote’ liner should attenuate the sound propagating over the liner between the source and the observer; the ‘pressure side’ (PS) and ‘suction side’ (SS) are a combination of both. Note that this is an engineering approach since the exact location of the source in the top view is not clear and shielding effects may be present.

The PSD reduction measured with the far-field array in the pressure side ($(\phi, \theta) = (0, -90)$ deg.) and in the suction side ($(\phi, \theta) = (0, +45)$ deg.) is shown in Fig. 16a and Fig. 16b respectively. As in previous figures, the results have been filtered with a Savitzky–Golay filter to smooth the data while maintaining the general trends. Only the data up to 12 kHz is shown because above that frequency the reduced noise levels approach those of the background noise and hence all liner configurations exhibit a similar performance.

The PSD reduction measured on the pressure side position (Fig. 16a) is similar for all configurations up to approximate 9.5 kHz. The following points can be drawn from the results in the gap noise dominated frequency range (9-12 kHz): (1) the PS liner (green) has the closest performance to the full liner (black), as expected since the measurements are made from a PS position; (2) the SS liner (magenta) and the local liner (blue) have also a similar performance, which also is expected for the same reason; (3) the remote liner (red) has the lowest noise reduction, which could suggest that a potential source modification effect present in the other configurations is missing in the remote liner configuration.

The same analysis is now followed for the measurements on the suction side position (Fig. 16b), focused again on the gap noise dominated frequency range (9-12 kHz) due to the small variations in the noise reductions of the various liner configurations at lower frequencies. Two unexpected effects can be observed: (1) the remote liner (red) has the best performance and practically the same as the SS liner (magenta) at the higher frequencies, suggesting that source modification benefits are not present, in contrast to the data from the pressure side (Fig. 16a); (2) the PS liner (green) has similar but better performance than the local liner (blue), which is also unexpected since the sound travels over the same lined surface from the source to the receiver.

In summary, the measurements taken on the pressure side may suggest some weak source modification effects but the data from the suction side is inconclusive. Measurements averaged over a range of meridian positions could give a better picture of the problem and account for any changes in directivity induced by the different liner configurations. Additional measurements of the unsteady pressure fluctuations on the airfoil surface for a hard wall case and with the over-tip liner could give more insight on source modification effects that may occur due to the presence of the lined surface.

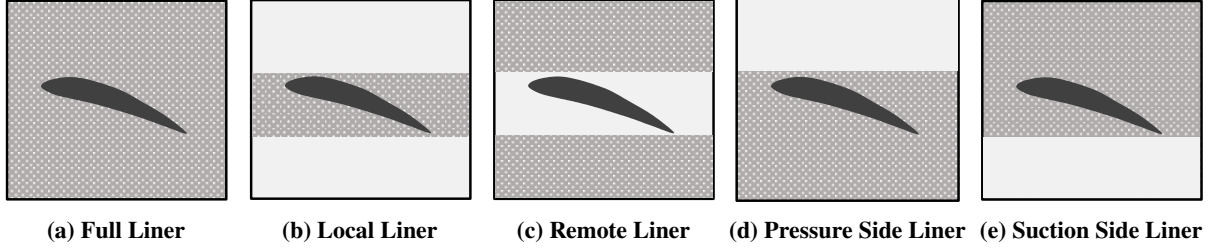


Fig. 15 Liner configurations tested for the source modification tests.

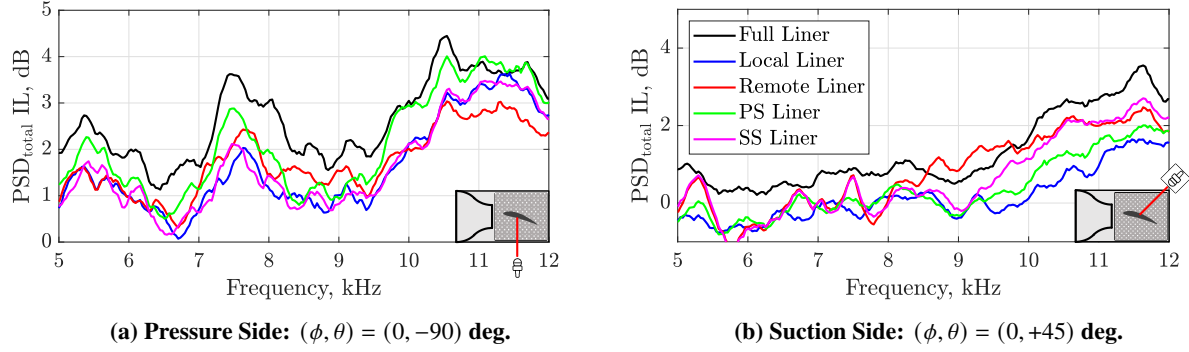


Fig. 16 Measured noise PSD reductions for different over-tip liners.

D. Use of TE feathers

The effects of trailing edge feathers is considered next. The motivation behind the use of TE feathers is to reduce the contribution of TEN such that the dominant noise sources are located nearer the tip of the airfoil, and hence more prone to over-tip liner noise reductions. Note that the feathers are not installed along the full span of the airfoil section, leaving the area near the tip with the baseline trailing edge. Besides, the liner configuration with wire mesh ID7 has been manufactured with a shallower cavity depth of 13 mm to move the first anti-resonance of the liner towards higher frequencies (~ 13 kHz) and to avoid a local minimum in the noise reduction spectra at frequencies of interest. The results are presented for a fixed gap size of $e = 5$ mm, AoA = 18 deg. and S3.

The power from the full domain and the equivalent power radiated from GAPB are shown in Fig. 17a and Fig. 17b respectively. The four curves correspond to: (1) the hard wall reference case with baseline or standard TE (BL), (2) the hard wall reference case but with feathered TE (TEF), (3) the lined configuration with BL and (4) the lined configuration with TEF. The corresponding PWL maps for the frequency range $f=[6-9]$ kHz, for which TEF are most effective, are shown in Fig. 17c-17f. The effect of the TEF is most clearly seen in Fig. 17a for $f=[6-9]$ kHz, with a drastic reduction of the TEN hump for both hard and lined configurations, which is also observed in the PWL maps. A smaller but still significant effect of the TEF is present in the gap region, as shown in Fig. 17b. The spectra is dominated by gap noise for frequencies over 9 kHz and the use of the baseline or feathered trailing edge does not make any difference, both configurations now collapsing to the hard/lined solution.

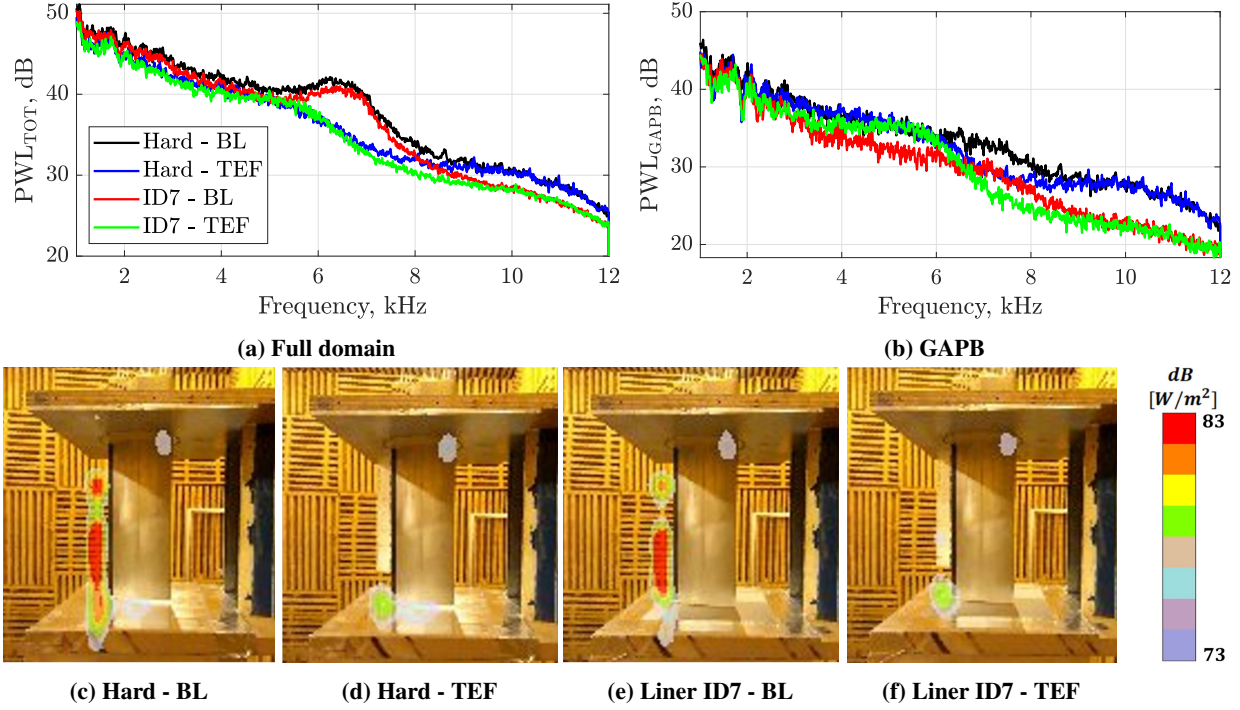


Fig. 17 Noise localization and extraction for the baseline (BL,(c) and (e)) and feathered (TEF, (d) and (f)) trailing edged configurations. The PWL maps are rendered for the frequency range of $f=[6-9]$ kHz.

The gap noise generated by the tip leakage flow and the noise reduction by the over-tip liner can be quantified following an analogous procedure to that in Section V. These are compared with the baseline and feathered trailing edges in Fig. 18. Tip gap noise is not affected by the use of TE feathers (Fig. 18a). That is unlikely to occur if the treatment were extended to the tip of the airfoil since one of the main noise generation mechanisms would be modified. The liner noise reduction is also found to be little affected by the trailing edge treatment in the frequencies dominated by gap noise, although a local minimum around 5.5 kHz can be seen for the TEF configuration in Fig. 18b. This analysis is based on the PWL extracted from the measurements of the spiral array but the same trends in terms of PSD levels and reductions have been found from the far-field measurements made on the suction side of the airfoil. However, the noise reduction minimum at 5.5 kHz does not appear on the pressure side ($\theta = -90$ deg.) and the same performance is observed for the baseline and feathered trailing edged configurations. The results presented here reinforce the point made in Section V that over-tip liners reduce the noise sources located close to the liner regardless of the noise generation mechanism.

VII. Comparison with point source analytical model

Analytical methods to model the tip gap noise generated by the turbulent eddies in the cross-flow as they are scattered by the tip suction side edge and trailing edge have been explored previously [23]. A modified version of Amiet's theory [24] with spanwise attenuation to damp the perturbations away from the tip was suggested for the former mechanism and an adaptation of Dunne and Howe's [25] model of a vortex through a tip clearance gap for the latter. Neither of

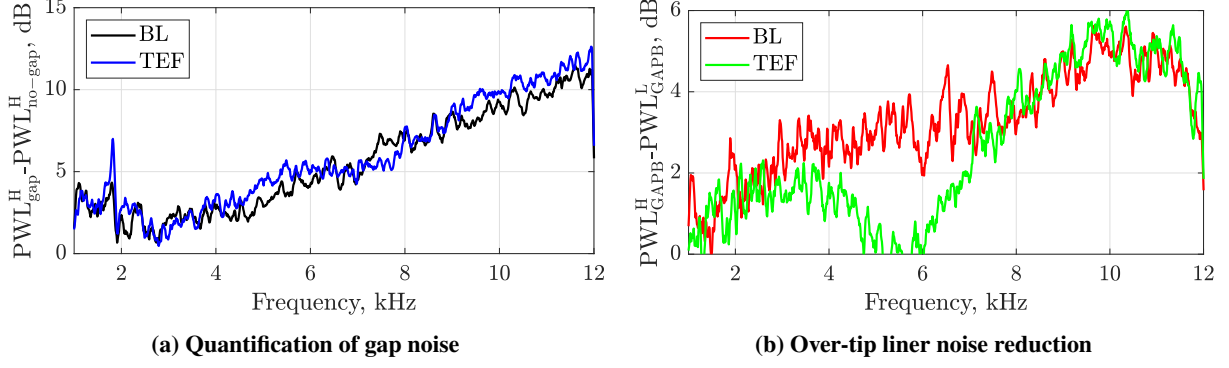


Fig. 18 Quantification of the gap noise generated by the tip leakage flow and PWL noise reductions by the over-tip liner in GAPB for the baseline (BL) and feathered (TEF) trailing edged configurations.

these methods is applicable here because our focus is not on the noise generation itself but the noise suppression by over-tip liners. Instead, a simpler approach based on a point source located over an infinite hard/lined plane has been used. (Again here we use the $e^{j\omega t}$ -convention).

The analytical model presented in this section is an adaptation of the Thomasson [26] formulation of the pressure field of a monopole source over a lined surface in the form presented in [27]. The total pressure field is a superposition of the direct field radiated by the source p_S , by the image source p_I and a correction to account for the lined boundary condition of the surface p_C . Expressed in cylindrical coordinates (r, z) , where r is the radius in the (x, y) plane, that is

$$p(r, z) = p_S(r, z) + p_I(r, z) + p_C(r, z) \quad , \quad (8)$$

with

$$p_S(r, z) = -\frac{1}{4\pi R_S} e^{-jkR_S} \quad , \quad (9)$$

$$p_I(r, z) = -\frac{1}{4\pi R_I} e^{-jkR_I} \quad , \quad (10)$$

where $R_S = |\mathbf{x}_R - \mathbf{x}_S|$ and $R_I = |\mathbf{x}_R - \mathbf{x}_I|$ with \mathbf{x}_R , \mathbf{x}_S and \mathbf{x}_I being the position in space of the receiver, the source and the image source respectively and k the wavenumber. The reflected contribution from the lined surface p_C is given by Eq. 11, the details of the derivation can be found in [26, 27].

$$p_C = \begin{cases} p_{SD} + p_B & \text{if } \text{Re}(\gamma_1) < -1 \quad \text{and } \text{Im}(A) > 0 \\ p_{SD} & \text{otherwise} \end{cases} \quad , \quad (11)$$

with

$$p_{SD} = -\frac{kA}{2\pi} e^{-jkR_I} \int_{t=0}^{+\infty} \frac{e^{-kR_I t}}{\sqrt{(-1+jt-\gamma_0)(-1+jt-\gamma_1)}} dt \quad , \quad (12)$$

$$p_B = \frac{kA}{2} H_0^{(2)} \left(kr\sqrt{1-A^2} \right) e^{jk(z+e)A} \quad , \quad (13)$$

where

$$\gamma_0 = A \cos \theta_0 + \sqrt{1-A^2} \sin \theta_0 \quad , \quad (14)$$

$$\gamma_1 = A \cos \theta_0 - \sqrt{1-A^2} \sin \theta_0 \quad , \quad (15)$$

$$t_1 = \frac{\text{Im} [(\gamma_0 + 1)(\gamma_1 + 1)]}{\text{Re} [(\gamma_0 + 1) + (\gamma_1 + 1)]} \quad , \quad (16)$$

e is the vertical distance from the source to the plane, $A = 1/Z$ the admittance of the lined plane and θ_0 the angle between the the z-axis and $\mathbf{R}_I = \mathbf{x}_R - \mathbf{x}_I$. As indicated in the literature [26], the square root in Eq. 12 is taken with a negative real part unless the conditions (1) $\text{Re}(\gamma_1) < -1$, (2) $\text{Im}(A) > 0$ and (3) $t > t_1$ are simultaneously fulfilled.

A prediction of the PSD IL can be obtained by assuming that the sources are concentrated at the airfoil tip, hence separated vertically from the surface by the gap size e , and making use of Eq. 8 with the coordinates of the receiver as the relative locations of the far-field microphones. The model can be numerically extended to dipoles and quadrupoles by considering monopole sources of opposite phase separated by a distance ϵ such that $\epsilon \ll \lambda$ and $\epsilon \ll e$, as indicated in the third column of Table 2.

The computation of the power radiated by a point source over a hard/lined plane across an arbitrary surface S in space is required to obtain an analytical prediction comparable with the measured PWL IL. In particular, it should be possible to integrate the intensity field through the surface of the spiral array used in the experimental set-up, as indicated in Fig. 19b. The computational domain has been discretised to allow for a numerical approximation of the acoustic particle velocity component normal to the surface of the spiral array (u_x) and the associated acoustic intensity (I_x):

$$u_x(x, y, z) = \frac{j}{\rho c k} \frac{p(x + \Delta x, y, z) - p(x, y, z)}{\Delta x} \quad , \quad (17)$$

$$I_x(x, y, z) = \frac{1}{2} \text{Re} \left(p(x, y, z) u_x^*(x, y, z) \right) \quad , \quad (18)$$

and for numerical integration of the acoustic intensity over the spiral array to obtain the acoustic power:

$$P = \int_S I_x dS = \sum_i \sum_j I_x(x, y_i, z_j) \Delta y \Delta z \quad . \quad (19)$$

The numerical procedure described above is verified with analytical models available in the literature. The case of a static point source (monopole, dipole and quadrupole) over an infinite rigid plane was considered by Ingard and Lamb [28]. Their analysis was based in the use of the method of images and the power output obtained by integrating the energy flux away from the source. They gave explicit analytical power amplification factors, defined as the ratio of power radiated in the presence of the plane (P) to the power radiated in free-field (P_f). A summary of the analytical expressions is shown in Table 2, where $z = 2ke$. An alternative approach was introduced by Levine [29], consisting of a direct evaluation of a secondary source at the source position to account for the presence of the surface. He applied this method for a monopole point source with several plane and half-plane configurations, including an infinite lined plane. The power amplification factor corresponding to the power radiated *away* from the surface is expressed as

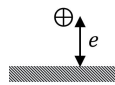
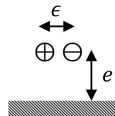
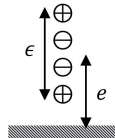
$$\frac{P}{P_f} = 1 + \frac{\sin z}{z} + 2\text{Re} \left(A e^{jAz} [E_1(j[1+A]z) - E_1(jAz)] \right) - 2\text{Re}(A) \int_0^1 \frac{\mu d\mu}{|A + \sqrt{1-\mu^2}|^2} \quad , \quad (20)$$

where $z = 2ke$ as before and $E_1(\zeta)$ is defined as the integral

$$E_1(\zeta) = \int_{\zeta}^{\infty} \frac{e^{-\xi} d\xi}{\xi}, \quad |\arg(\zeta)| < \pi \quad . \quad (21)$$

If the admittance is set to zero (hard wall), the expression is consistent with that in Table 2.

Table 2 Summary of Ingard and Lamb [28] power amplification factors for a point source in the presence of a rigid plane and diagrams of the discrete models used for each type of point source.

Source	Power amplification factor	Discrete Model
Monopole	$\frac{P}{P_f} = 1 + \frac{\sin z}{z} \quad (22)$	
Dipole (horizontal)	$\frac{P}{P_f} = 1 + \frac{3}{z} \left[\frac{\sin z}{z^2} - \frac{\cos z}{z} \right] \quad (23)$	
Quadrupole (longitudinal, vertical)	$\frac{P}{P_f} = 1 + \frac{5}{z} \left[\left(1 - \frac{12}{z^2} + \frac{24}{z^4} \right) \sin z + \left(\frac{4}{z} - \frac{24}{z^3} \right) \cos z \right] \quad (24)$	

The power obtained by integration of the intensity field through the hemi-sphere above the half-space is required to

compare the proposed procedure with the exact analytical expressions: Eq. 20 for a monopole over a lined plane and Eq. 22-24 for multipoles over a rigid surface. It is convenient to express the acoustic field in spherical coordinates for this verification exercise outlined in Fig. 19a. The comparison of the computed numerical amplification factors with the exact solution is shown in Fig. 20 for three values of liner impedance. The results are plotted as a function of e/λ : the gap size (e) normalised with the wavelength (λ). Note that the power output of the point source can be drastically reduced when located very close to the lined surface (relative to the wavelength): from $0.6P_f$ at $e/\lambda=2$ to $0.2P_f$ at $e/\lambda=0.01$ for $Z = 1$ (Fig. 20b). Hence, the significant predicted variability of the PSD IL and PWL IL for different gap sizes shown in Fig. 22. An analogous comparison to verify the discrete model used for multipole sources is shown in Fig. 21 for a hard wall plane. The results also present an excellent agreement and show the well-known result that the point source radiates twice the power when $e = 0$ (due to the image source) and tends to the free-field values as it moves away from the surface.

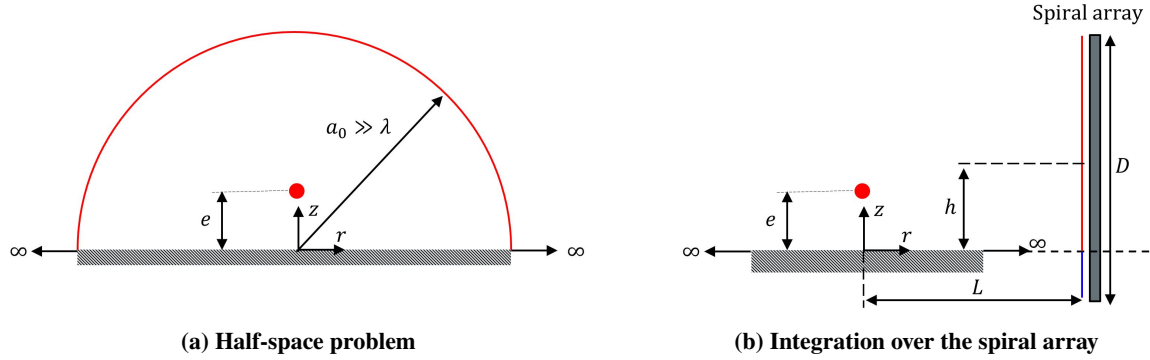


Fig. 19 Geometries used for (a) the verification of the source power computation and (b) the comparison with the post-processed spiral array data.

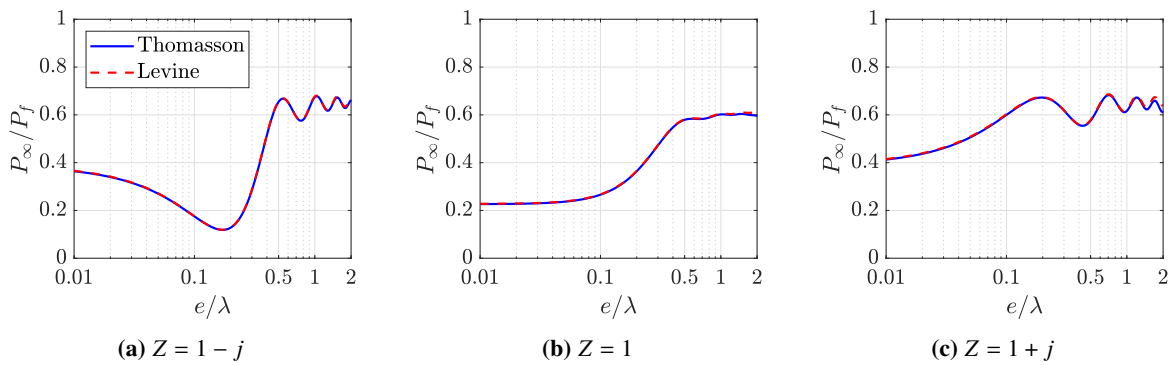


Fig. 20 Verification of the discrete numerical integration for the power output of a monopole source over a lined infinite plane.

The predicted PSD IL evaluated at the far-field microphone position $(\phi, \theta) = (0, -90)$ deg. for a dipole normal to the chord of the airfoil (AoA=18 deg.) and located at the TE is shown in Fig. 22a. The three humps of PSD insertion loss (IL) with the resonances and anti-resonances are of course captured by the analytical model. The trend of lower

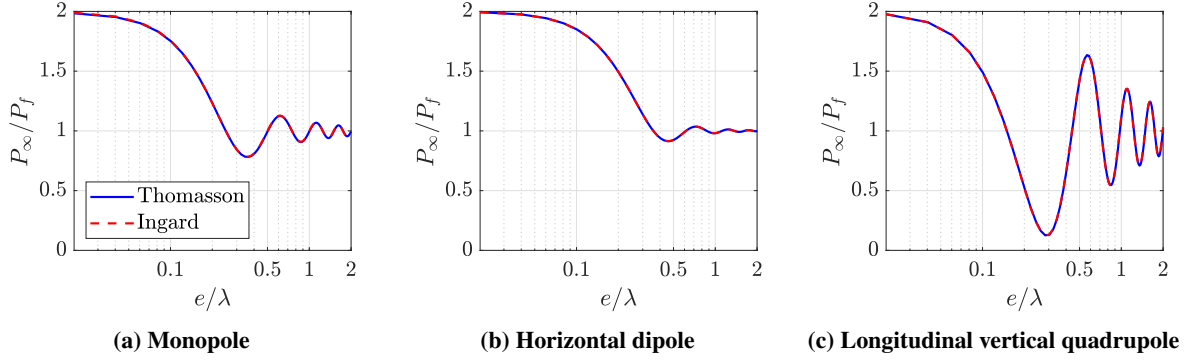


Fig. 21 Verification of the discrete model for the power output of multipole sources over a hard infinite plane.

IL as the gap size is increased can be clearly observed here and the rate of the loss of performance with the gap size increases with frequency: at 5 kHz ~ 7 dB less IL is predicted when the gap size changes from 5 mm to 25 mm whereas at 10 kHz the variation is of ~ 10 dB and at 20 kHz soars up to 15 dB. The resonance peaks become higher but narrower as the gap size increases, causing the trends outlined here and observed in Section VI.B. The same conclusions can be drawn from the PWL IL predictions shown in Fig. 22b, which are directly comparable to the PWL IL extracted from GAPB shown in Fig. 14b.

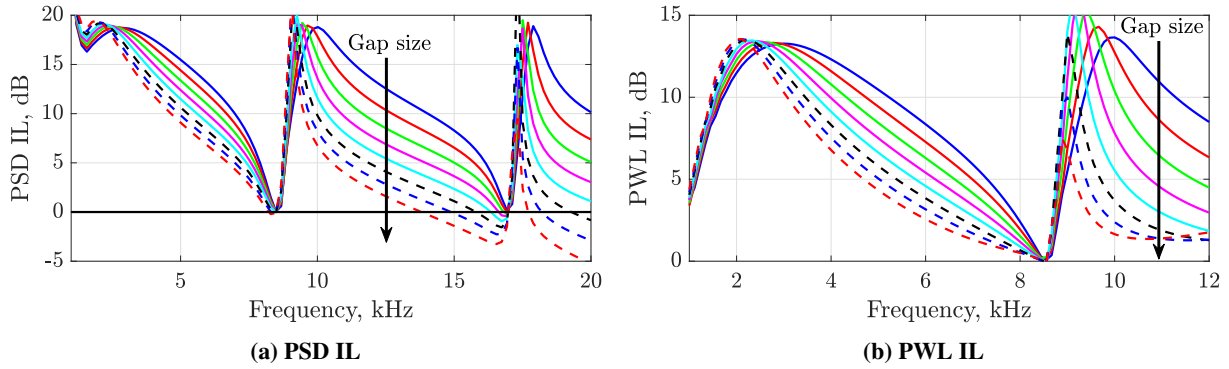


Fig. 22 Predicted (a) PSD and (b) PWL gap noise reduction for different gap sizes and a dipole perpendicular to the airfoil chord.

A comparison of the predicted PSD IL assuming different types of point source with the measured isolated gap noise PSD_{gap} IL is shown in Fig. 23 for a selection of gap sizes. Although the peak IL is generally overestimated, a fairly good agreement in the magnitude and spectral shape can be observed for the rest of the spectrum, especially in the second and third humps of noise reduction. The experimental results follow the trend of lower broadband noise reduction as the gap size increases and the agreement with the prediction gets better for bigger gaps, which can be linked to a stronger and more localised source. The spectral shape of the predicted PSD of a monopole and a dipole are very different, but they collapse when performing the subtraction to obtain the PSD IL. The quadrupole has a lower noise reduction as expected and would only be a candidate to represent the physical mechanisms if a jet-type source was measured. Based on the

scaling of gap noise with the free-field velocity discussed in Section VI.A, a dipole-type source is the best candidate.

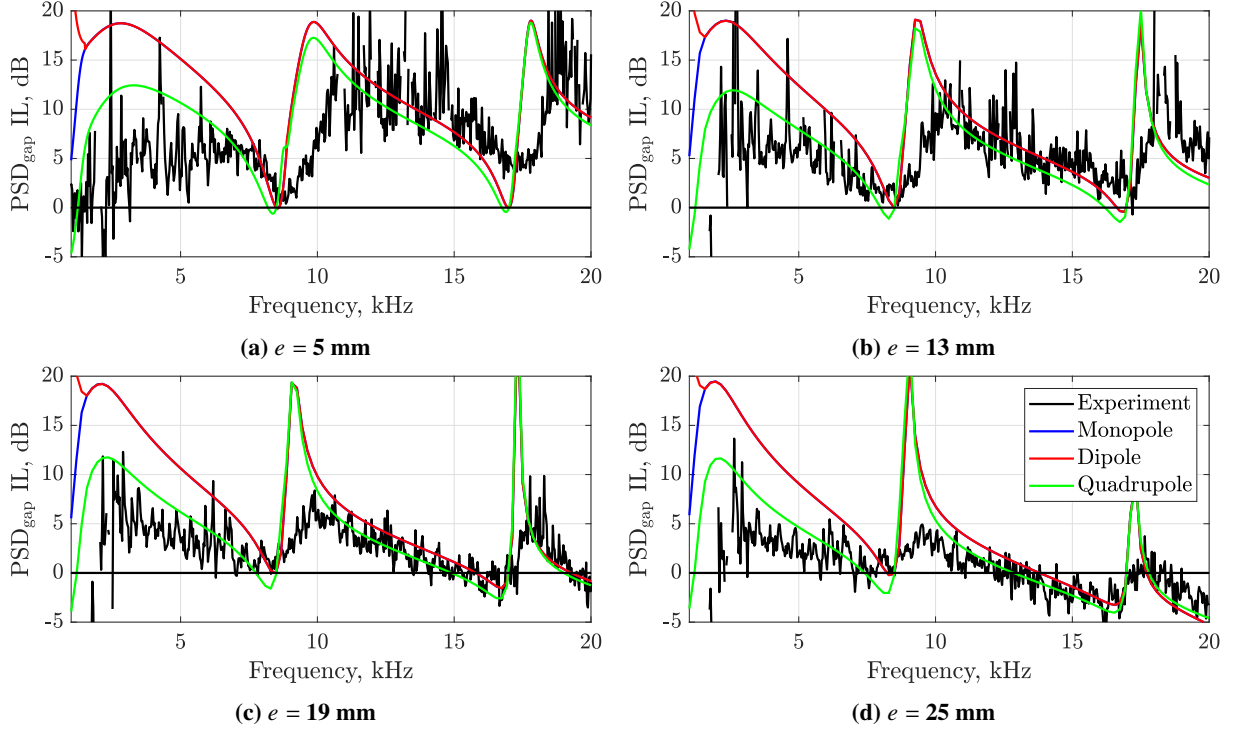


Fig. 23 Measured and predicted gap noise PSD IL for different gap sizes.

An equivalent comparison is made in Fig. 24 between the predicted PWL IL evaluated over the surface of the spiral array, and the PWL IL from the GAPB area extracted using the post-processing of the spiral array data. The prediction also overestimates the peak PWL IL but a better agreement than with the PSD IL is found at lower frequencies. Again, the predicted and measured data are closer for higher gap sizes and the monopole and dipole present a good agreement both in magnitude and spectral shape for almost the full frequency range in Fig. 24c and 24c. The quadrupole source, as expected, is not a good candidate for the modelling of gap noise reduction in the current experiment as observed with large differences with the measured data as the gap size is increased.

VIII. Conclusions

This work has focused on improving the understanding of the physical mechanisms of noise reduction of the Over-Tip-Rotor (OTR) liner concept by means of a wind tunnel experiment. The experiment consisted of a static airfoil mounted vertically between two flat plates and separated from the lower one by a small gap. The pressure difference between the suction side and the pressure side of the airfoil creates a jet-like flow through the tip gap that resembles the noise generation mechanism of a tip vortex. A hard wall or a SDOF liner insert is flush mounted in the lower plate representing an over-tip liner. Differences of measured far-field sound spectra and sound power from spiral microphone-array measurements have been used to isolate and quantify gap noise and the noise reduction benefits of

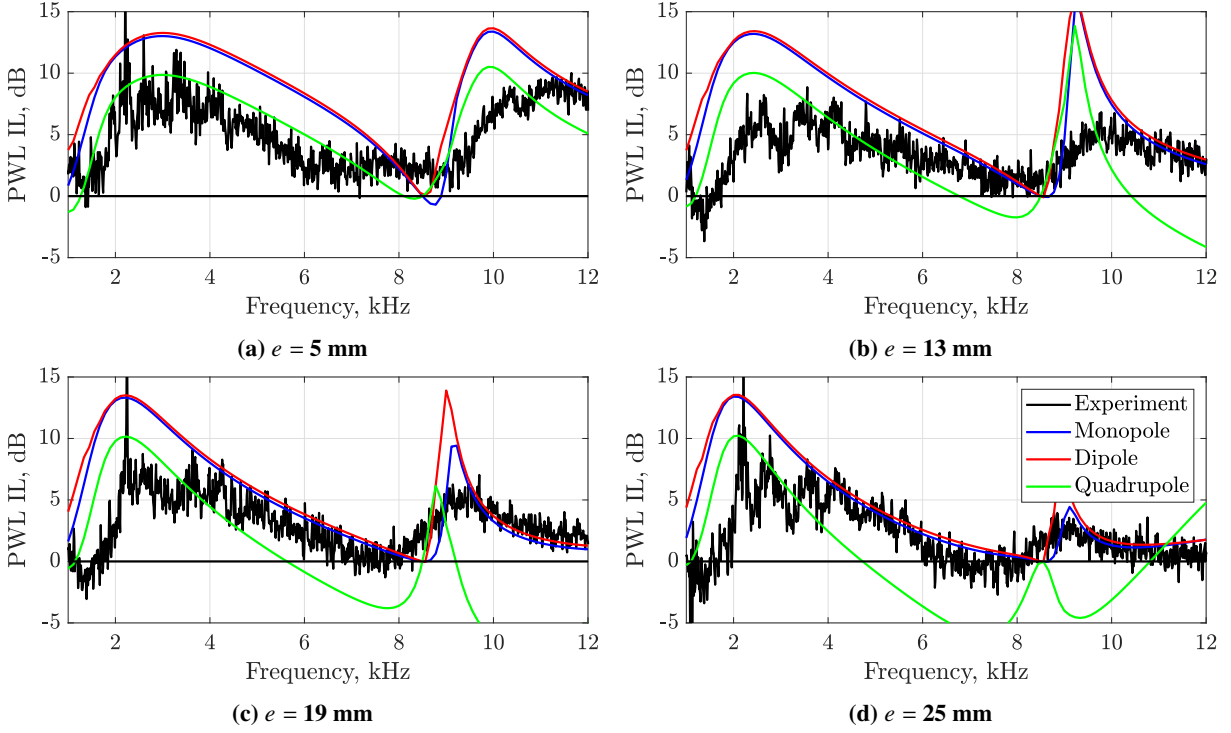


Fig. 24 Measured and predicted gap noise PWL IL for different gap sizes.

over-tip liners.

Source localization results from the spiral array show that the over-tip liner reduces the noise radiated in the vicinity of the liner, which can be dominated by gap noise or trailing edge noise depending on the frequency range. The over-tip liner gap noise reduction spectra obtained using differences of far-field sound spectra and differences of source-power spectra show peak broadband reduction of gap noise by 5-10 dB, corresponding to 2-3 dB of noise reduction in the full domain. It has been found that the performance of the over-tip liner is not significantly modified by the tip-leakage flow, which suggests that the liner suppresses the noise sources located in its vicinity, irrespective of the dominant source (i.e. TE or gap noise sources). This result highlights the potential of over-tip liners in turbo-machinery applications even if the role of gap noise is not fully quantified.

A series of parametric studies have been presented: the scaling of gap noise with the free-stream velocity; the directivity of the dominant sources; the effect of gap size in gap noise generation and the noise reduction of the over-tip liner; modified lined configurations to study source modification effects and the use of trailing edge feathers.

The results suggest that the interaction of turbulence with the tip edges is the dominant source of gap noise in the current tests, with a PSD dependence of the 5^{th} power of the free-stream velocity. The gap noise generally increases with the gap size, although it can saturate at low frequencies ($f < 6$ kHz) and remain unaffected at high frequencies ($f > 12$ kHz).

Noise reduction benefits of the over-tip liner are reduced when increasing the gap size, in agreement with the

prediction model evaluated here. Measurements with various liner configurations might suggest weak source modification effects but the results are inconclusive and most of the noise reduction is attributable to the conventional attenuation of the sound waves propagating over the lined surface.

The use of TE feathers concentrate the dominant noise sources towards the tip of the airfoil for an extended range of frequencies and the results reinforce the point that over-tip liners attenuate the noise sources located close to the liner regardless of the noise generation mechanism.

An analytical prediction model for the over-tip liner noise reduction has been proposed. It is based on a discrete evaluation of Thomasson formulation [26] for a monopole point source located over an infinite lined plane. The scheme used to compute the power radiated by multipole sources over hard/lined surfaces is verified by comparison with exact solutions given by Ingard and Lamb [28] and Levine [29]. A comparison of the predicted and measured gap noise PSD IL and PWL IL for various gap sizes has shown that, although the peak IL is usually overestimated, a reasonable agreement both in magnitude and spectral shape can be obtained, the match improving for larger gap sizes.

Acknowledgments

This project is funded by the European Union's Horizon 2020 research and innovation programme under a Marie Skłodowska-Curie Innovative Training Network (ITN) grant (Agreement No 722401) within the SmartAnswer consortium. The tests were performed within the framework of the Labex CeLyA of the Université de Lyon, within the programme 'Investissements d'Avenir' (ANR-10-LABX-0060/ANR-11-IDEX-0007) operated by the French National Research Agency (ANR). The authors would like to thank Prof. Michel Roger for his support and insight in all the stages of the investigation and to Dr. Pascal Souchotte for the use of the materials and the experimental facilities at ECL. The authors would also like to thank Dr. Paul Murray for his suggestions in the design of the liners and to Dr. Chaitanya Paruchuri for the interesting discussions on the analysis of the results.

References

- [1] Jacob, M. C., Grilliat, J., Camussi, R., and Gennaro, G. C., "Aeroacoustic investigation of a single airfoil tip leakage flow," *International Journal of Aeroacoustics*, Vol. 9, No. 3, 2010, pp. 253–272. doi:<https://doi.org/10.1260/1475-472X.9.3.253>.
- [2] Grilliat, J., Jacob, M., Camussi, R., and Caputi-Gennaro, G., "Tip Leakage Experiment - Part One: Aerodynamic And Acoustic Measurements," *13th AIAA/CEAS Aeroacoustics Conference*, 2007. doi:<https://doi.org/10.2514/6.2007-3684>.
- [3] Boudet, J., Jacob, M. C., Caro, J., Jondeau, E., and Li, B., "Wavelet analysis of a blade tip-leakage flow," *AIAA Journal*, Vol. 56, No. 8, 2018, pp. 3332–3336. doi:<https://doi.org/10.2514/1.J056703>.
- [4] Koch, R., Sanjose, M., and Moreau, S., "Large-Eddy Simulation of a Single Airfoil Tip-Leakage Flow," *AIAA AVIATION Forum*, 2020. doi:<https://doi.org/10.2514/6.2020-2514>.

- [5] Peake, N., and Parry, A. B., “Modern Challenges Facing Turbomachinery Aeroacoustics,” *Annual Review of Fluid Mechanics*, 2011, pp. 227–250. doi:<https://doi.org/10.1146/annurev-fluid-120710-101231>.
- [6] Sutliff, D. L., Elliott, D. M., Jones, M. G., and Hartley, T. C., “Attenuation of FJ44 turbofan engine noise with a foam-metal liner installed over-the-rotor,” *15th AIAA/CEAS Aeroacoustics Conference*, 2009. doi:<https://doi.org/10.2514/6.2009-3141>.
- [7] Elliott, D., Woodward, R., and Podboy, G., “Acoustic Performance of Novel Fan Noise Reduction Technologies for a High Bypass Model Turbofan at Simulated Flight Conditions,” *15th AIAA/CEAS Aeroacoustics Conference (30th AIAA Aeroacoustics Conference)*, 2009. doi:<http://arc.aiaa.org/doi/abs/10.2514/6.2009-3140>.
- [8] Sutliff, D. L., and Jones, M. G., “Low-Speed Fan Noise Attenuation from a Foam-Metal Liner,” *Journal of Aircraft*, Vol. 46, No. 4, 2009, pp. 1381–1394. doi:<http://arc.aiaa.org/doi/10.2514/1.41369>.
- [9] Sutliff, D. L., Jones, M. G., and Hartley, T. C., “High-Speed Turbofan Noise Reduction Using Foam-Metal Liner Over-the-Rotor,” *Journal of Aircraft*, Vol. 50, No. 5, 2013, pp. 1491–1503. doi:<http://arc.aiaa.org/doi/10.2514/1.C03202>.
- [10] Gazella, M. R., and Tester, B. J., “Evaluating the Acoustic Benefits of Over-the- Rotor Acoustic Treatments Installed on the Advanced Noise Control Fan,” *AIAA/CEAS Aeroacoustics Conference*, 2017. doi:10.2514/6.2017-3872.
- [11] Bozak, R., and Dougherty, R. P., “Measurement of Noise Reduction from Acoustic Casing Treatments Installed Over a Subscale High Bypass Ratio Turbofan Rotor,” *AIAA/CEAS Aeroacoustics Conference*, 2018. doi:<https://arc.aiaa.org/doi/10.2514/6.2018-4099>.
- [12] Bozak, R., Hughes, C., and Buckley, J., “The Aerodynamic Performance of an Over-The-Rotor Liner with Circumferential Grooves on a High Bypass Ratio Turbofan Rotor,” Tech. rep., 2013. URL <https://ntrs.nasa.gov/archive/nasa/casi.ntrs.nasa.gov/20140001135.pdf>.
- [13] Bozak, R. F., and Podboy, G. G., “Evaluating the Aerodynamic Impact of Circumferentially Grooved Fan Casing Treatments With Integrated Acoustic Liners on a Turbofan Rotor,” *Proceedings of ASME Turbo Expo 2019*, 2019, pp. 1–11. doi:<https://doi.org/10.1115/GT2019-91369>.
- [14] Zhang, W., Wang, X., Du, L., and Sun, X., “Mutual effect between swept-and-leaned vanes and acoustic liners on fan interaction-noise reduction,” *AIAA Journal*, Vol. 57, No. 6, 2019, pp. 2479–2488. doi:<https://arc.aiaa.org/doi/10.2514/1.J057854>.
- [15] Palleja-Cabre, S., Tester, B. J., Astley, R. J., and Bozak, R., “Modelling of Over-The-Rotor Acoustic Treatments for Improved Noise Suppression in Turbofan Engines,” *25th AIAA/CEAS Aeroacoustics Conference*, 2019. doi:<https://doi.org/10.2514/6.2019-2580>.
- [16] Yakhina, G. R., Roger, M., Finez, A., Bouley, S., Baron, V., Moreau, S., and Giez, J., “Localization of Swept Free-Tip Airfoil Noise Sources by Microphone Array Processing,” *AIAA Journal*, 2020, pp. 1–12. doi:<https://doi.org/10.2514/1.J058231>.
- [17] Bampanis, G., and Roger, M., “Three-dimensional effects in the reduction of turbulence-impingement noise of aerofoils by wavy leading edges,” *Euronoise*, Vol. 1, 2018, pp. 97–104.

- [18] Bampanis, G., Roger, M., Ragni, D., Avallone, F., and Teruna, C., “Airfoil-Turbulence Interaction Noise Source Identification and its Reduction by Means of Leading Edge Serrations,” *25th AIAA/CEAS Aeroacoustics Conference*, 2019, pp. 1–18. doi:<https://doi.org/10.2514/6.2019-2741>.
- [19] Bampanis, G., “Three-Dimensional Aspects of Airfoil Turbulence-Impingement Noise and its Reduction by porous cells or wavy leading-edge,” Ph.D. thesis, University of Lyon, 2021.
- [20] Mottsigner, R. E., and Kraft, R. K., “Design and Performance of Duct Acoustic Treatment,” *Aeroacoustics of Flight Vehicles: Theory and Practice. Vol. 2: Noise Control*, 1991.
- [21] Piet, J.-F., and G.Elias, “Modelisation du champ acoustique incident sur la coiffe d’ariane 5 par des sources simples,” *Office National D’Études et de Recherches Aérospatiales Rept. TAP-94-062*, 1994.
- [22] Palreja-Cabre, S., “Fan proximity acoustic treatments for improved noise suppression in turbofan engines,” Ph.D. thesis, University of Southampton, 2021.
- [23] Grilliat, J., Jondeau, E., Jacob, M. C., Roger, M., and Camussi, R., “Broadband noise prediction models and measurements of tip leakage flows,” *14th AIAA/CEAS Aeroacoustics Conference (29th AIAA Aeroacoustics Conference)*, 2008. doi: <https://arc.aiaa.org/doi/abs/10.2514/6.2008-2845>.
- [24] Amiet, R. K., “Noise due to turbulent flow past a trailing edge,” *Journal of Sound and Vibration*, Vol. 47, No. 3, 1976, pp. 387–393. doi:[https://doi.org/10.1016/0022-460X\(76\)90948-2](https://doi.org/10.1016/0022-460X(76)90948-2).
- [25] Dunne, R. C., and Howe, M. S., “Wall-bounded blade-tip vortex interaction noise,” *Journal of Sound and Vibration*, Vol. 202, No. 5, 1997, pp. 605–618. doi:<https://doi.org/10.1006/jsvi.1996.0791>.
- [26] Thomasson, S., “Reflection of waves from a point source by an impedance boundary,” *J. Acoust. Soc. Am.*, Vol. 59, 1976, p. 780. doi:<https://doi.org/10.1121/1.380943>.
- [27] Coyette, J.-P., and Van den Nieuwenhof, B., “A conjugated infinite element method for half-space acoustic problems,” *The Journal of the Acoustical Society of America*, Vol. 108, No. 4, 2000, pp. 1464–1473. doi:<https://doi.org/10.1121/1.1289921>.
- [28] Ingard, U., and Lamb, G. L., “Effect of a Reflecting Plane on the Power Output of Sound Sources,” *The Journal of the Acoustical Society of America*, Vol. 29, No. 6, 1957, pp. 743–744. doi:<https://doi.org/10.1121/1.1909034>.
- [29] Levine, H., “Output of acoustical sources,” *J. Acoust. Soc. Am.*, Vol. 67(6), No. 1980, 1980, pp. 1935–1946. doi:<https://doi.org/10.1121/1.384459>.